J. Fluid Mech. (1980), *vol.* 96, *part* 4, *pp.* 671–704
Printed in Great Britain

Experiments on stably and neutrally stratified flow over a model three-dimensional hill

By J. C. R. HUNT

Department of Applied Mathematics and Theoretical Physics,
University of Cambridge

AND W. H. SNYDER†

Meteorology and Assessment Division, Environmental Sciences Research Laboratory,
U.S. Environmental Protection Agency, Research Triangle Park, NC 27711

(Received 8 January 1979 and in revised form 7 June 1979)

This paper describes the flow structure observed over a bell-shaped hill with height h (the profile of which is the reciprocal of a fourth-order polynomial) when it was placed first in a large towing tank containing stratified saline solutions with uniform stable density gradients and second in an unstratified wind tunnel. (A similarly shaped model hill was also studied in a small towing tank.) Observations were made at values of the Froude number F ($\simeq U/Nh$) in the range 0·1 to 1·7 and at $F = \infty$, where U is the towing speed and N is the Brunt–Väisälä frequency, and at values of the Reynolds number from 400 to 275 000. For $F \lesssim 0{\cdot}4$, the observations verify Drazin's (1961) theory for low-Froude-number flow over three-dimensional obstacles and establish limits of applicability. For Froude numbers of the order of unity, it is found that a classification of the lee-wave patterns and separated-flow regions observed in two-dimensional flows also appears to apply to three-dimensional hills.

Flow-visualization techniques were used extensively in obtaining both qualitative and quantitative information on the flow structure around the hill. Representative photographs of dye tracers, potassium permanganate dye streaks, shadowgraphs, surface dye smears, and hydrogen-bubble patterns are included here. While emphasis is centred on obtaining a basic understanding of the flow around three-dimensional hills, the results are applicable to the estimation of air pollutant dispersion around hills.

1. Introduction

The flow patterns and velocity distributions around three-dimensional hills need to be better understood before one can even interpret measurements in the atmospheric boundary layer let alone make quantitative predictions of the velocity field and dispersion of pollutants from sources in this kind of complex terrain. The broad aspects of the structure of these stratified flows that one would like to understand are:

(*a*) whether streamlines from upwind impinge on the hill, go round the hill, or go over the top;

† On assignment from the National Oceanic and Atmospheric Administration, United States Department of Commerce.

0022–1120/80/4383–8360 $02.00

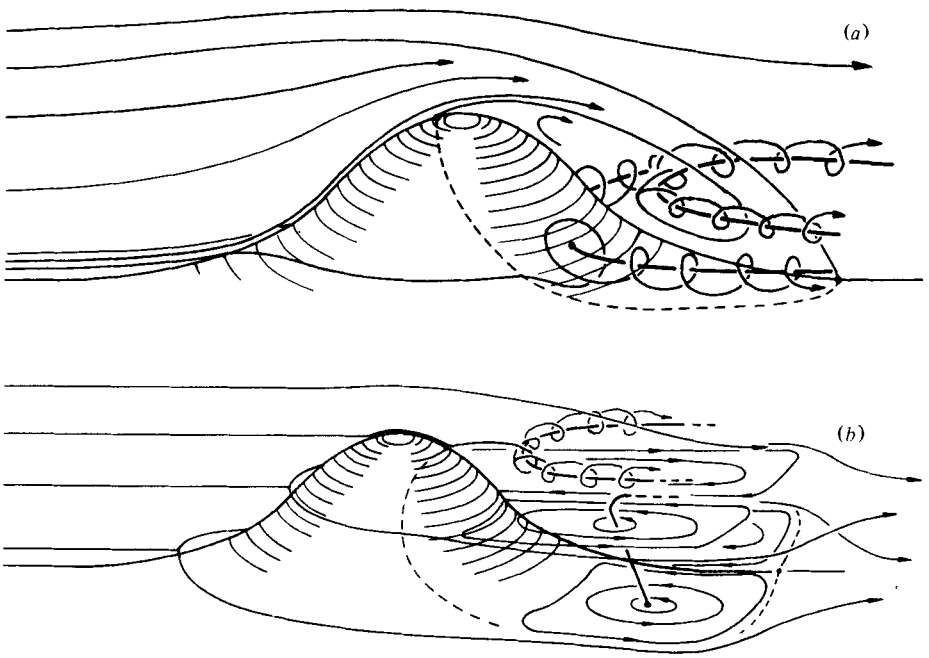

FIGURE 1. Sketch of flows over a three-dimensional hill in (*a*) neutral and (*b*) very stable stratification.

(*b*) the size and location of internal hydraulic jumps and the region of the separated or recirculating flow in the lee of the hill, as the stratification varies;

(*c*) the effects of heating and cooling of the surface.

Existing theory (see §2), model experiments (Brighton 1978; Riley, Liu & Geller 1976) and observations of air flow over mountains (Queney *et al.* 1960) all indicate that, when the stratification is strong enough, the air flows in approximately horizontal planes around the topography (see figure 1). This observation has been used in estimating surface concentrations caused by upwind sources of pollution (Hunt & Mulhearn 1973; Burt & Slater 1977). But hitherto there has been little firm laboratory or atmospheric data as to how *strong* the stratification must be for any given streamline starting below the top of the hill to pass round rather than over the hill. A criterion for this changeover to occur is suggested in §2 on the basis of the low-Froude-number theory of Drazin (1961), which the experiments described in §4 confirm. There has been no previous systematic experimental investigation of the flow around a three-dimensional surface obstacle as the Froude number is varied from much less to much greater than unity.

It is well known that a small amount of stratification can have a strong effect on the separated flow downwind of bluff obstacles such as hills or escarpments (see, for example, Scorer 1954, 1968). In the case of two-dimensional hills, the separation behind hills with moderate slopes can be suppressed, but 'rotors', in which there is reverse flow, may be found farther downwind as part of the lee-wave pattern. Internal hydraulic jumps are found downwind of hills with moderate or large slopes in which the streamlines jump abruptly upwards, the horizontal component of velocity decreases,

and a large amount of energy is dissipated. Despite its practical importance to air pollution dispersion and aeronautics, the distinctions and connexions among these phenomena are still far from clear, even in the case of two-dimensional hills. There has not even been a laboratory study of two-dimensional flows where all these phenomena occur, although some valuable insights were provided by the wind-tunnel study of Kitabayashi, Orgill & Cermak (1971) and the aircraft observations of Connell (1976) around Elk Mountain, Wyoming. If the slope of the hill is small enough, separation may occur without hydraulic jumps.

Recently the effects of stratification on separation have been studied by Brighton (1977) and Sykes (1978). Brighton performed a linear analysis of boundary-layer flow over ridges with small slopes which, by extrapolation, approximately indicates the location of and conditions for separation. Sykes' (1978) nonlinear numerical computations of laminar flow over a ridge could accurately predict the suppression and the onset of separation for a range of Froude numbers. Brighton (1977) also performed some *laminar flow* experiments in a stratified water channel at Cambridge which broadly confirmed his predictions. These results are discussed in more detail in § 2.

In this report, we describe laboratory studies of the flow patterns, with particular emphasis on the separated-flow regions and the internal hydraulic jumps, around a three-dimensional hill, axisymmetric about a vertical axis. A model hill with the shape of the inverse of a fourth-order polynomial has been studied in a large and a small stratified towing tank and in an unstratified wind tunnel. Several new techniques for flow visualization were developed during these experiments, which are described in § 3.

The method we adopt for analysing and presenting a large quantity of flow-visualization data of this kind is first to locate the points where the surface shear stresses are zero or where the velocity in a cross-section through the flow is zero. These points are then characterized in terms of whether they are separation or attachment points, and, more unusually, in terms of their *topological* nature as saddle points or node points, because topological theory (Hunt, Abell, Peterka & Woo 1978) shows that the number of saddle points in the surface-shear-stress lines must equal the number of node points. This provides a kinematic check on the inferred flow from the flow-visualization data. This minimal attempt at systematizing visualization data provides a more concrete basis for qualitative comparisons between (*a*) full-scale and model-scale observations of the flow around hills and (*b*) the theory and experiment.

Some quantitative results are also obtained from the flow-visualization experiments: namely, at low Froude number, the vertical deflexion of streamlines; at moderate to large Froude numbers, the distance of streamlines from the surface of the hill and the connexion between the lee waves and the separated flow downwind of the hill; and at large Froude numbers, the increase in velocity or speed-up over the hill.

As Scorer has pointed out, laboratory studies of stratified flows tend to overemphasize the effects of the upwind stratification rather than the equally, perhaps more, important effects of the local heating and cooling of the surface of the hills. These effects are not only local but may also have a large effect on the flow by inhibiting or promoting separation (Scorer 1968, p. 113; Brighton 1977). There have been some attempts to heat the surface of model terrain, but more to simulate fumigation of elevated plumes than katabatic or anabatic winds (Liu & Lin 1976). Any comparison between full-scale and model experiments, where such thermally generated winds are not simulated, must be made with great caution.

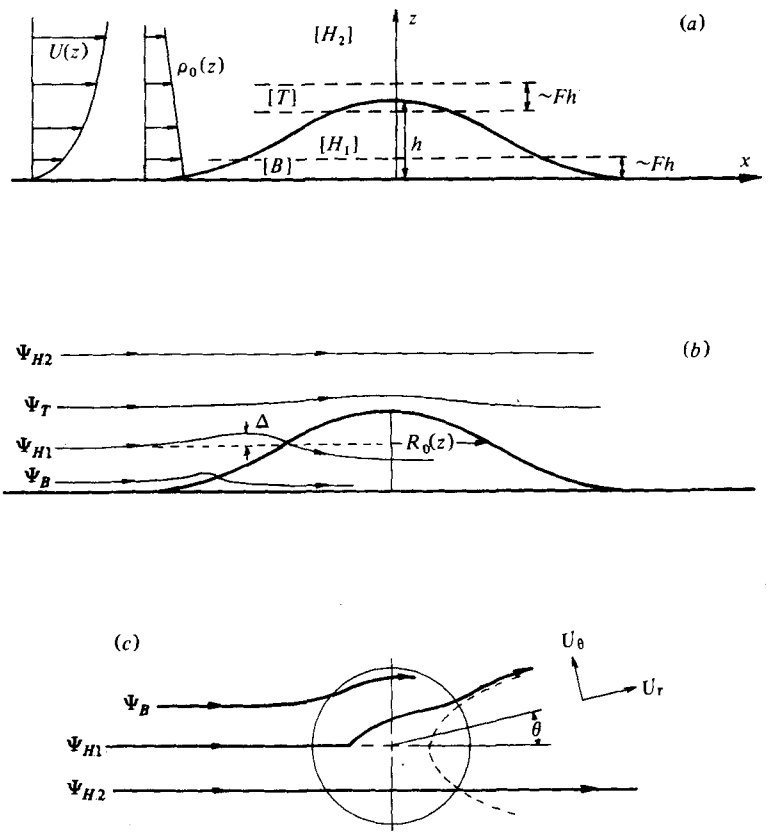

FIGURE 2. Small-Froude-number theory for flow over three-dimensional hills. (*a*) Definition of regions. (*b*) Streamline patterns. (*c*) Plan view.

In the interest of saving journal space, we have omitted many details. Additional photographs and more detailed descriptions of the apparatus and techniques are available in an EPA report by Hunt, Snyder & Lawson (1978), hereinafter referred to as HSL.

2. Review of theory

2.1. *Small-Froude-number theory*

The only theory giving quantitative results for stratified flow around a three-dimensional mountain or hill which is not merely a small perturbation of a plane surface is that due to Drazin (1961), which has been extended and largely confirmed experimentally by Riley *et al.* (1976) and Brighton (1978). The theory is valid asymptotically as the Froude number $F(= U(h)/Nh) \to 0$, where $U(h)$ is the upstream velocity at the level of the top of the hill, N is the Brunt–Väisälä frequency (i.e. proportional to the square root of the density gradient), and h is the height of the hill (see figure 2*a*). The essential results from our present understanding of the theory are the following.

(*a*) The fluid moves approximately horizontally in two regions: $[H_1]$, above the plane $z = 0$ and below the summit of the hill, and $[H_2]$, above the summit (see figure 2).

(*b*) Regions [B] and [T] exist at the base and the top of the hill with thicknesses $\alpha_B Fh$, and $\alpha_T Fh$,† where the α's are factors of order one and depend on the shape of the hill. (We assume that the α's are 1·0 unless otherwise stated, and that the extent of [T] is symmetrical above and below the summit.) In these regions, the flow is not constrained to move horizontally.

(*c*) In the lee of the hill there may be a wake in which the flow also moves approximately horizontally, but the streamlines in the wake may not emanate from the same levels upstream, or may not emanate from upstream at all.

(*d*) In [H_1], to the first approximation as $F \to 0$, the horizontal velocity

$$U_H = (U_r, U_\theta)$$

is described by potential theory; for example, if the mountain is axisymmetric about the z axis, with a radius $R_0(z)$, and if the wake is ignored,

$$U_r = U(z)\,(1 - R_0^2(z)/r^2)\cos\theta, \tag{2.1a}$$

and

$$U_\theta = -U(z)\,(1 + R_0^2(z)/r^2)\sin\theta. \tag{2.1b}$$

Riley *et al.* (1976) showed how the effect of the wake can be estimated by using free-streamline potential theory.

(*e*) It follows from (2.1) that the horizontal pressure gradients in [H_1] vary with z owing to U and R_0 variations, and, consequently, the vertical pressure gradient $(\partial p/\partial z)$ is perturbed. For example, on the stagnation line this perturbation (denoted by $\partial\hat{p}/\partial z$) is negative because dR_0/dz is negative. In strongly stratified flows, the perturbation pressure gradient is balanced by perturbations to the density gradient, which are produced by vertical displacements $\Delta(r,\theta)$ of streamlines starting from upstream. Generalizing Drazin's theory to allow for variations in $U(z)$, Brighton (1978) showed that

$$\Delta(r,\theta) = -(\partial\hat{p}/\partial z)/[g\,\partial\rho_0/\partial z],$$

or

$$\Delta(r,\theta) = -\frac{1}{2N^2}\left[\frac{\partial}{\partial z}(U^2 - (U_r^2 + U_\theta^2))\right]. \tag{2.2}$$

For the simple flow given by (2.1),

$$\Delta(r,\theta) = -\frac{1}{N^2}\left[\frac{dU^2(z)}{dz}\frac{R_0^2}{r^2}\left(\cos 2\theta - \frac{R_0^2}{2r^2}\right) + \frac{U^2}{r^2}\frac{d(R_0^2)}{dz}\left(\cos 2\theta - \frac{R_0^2}{r^2}\right)\right]. \tag{2.3}$$

The mean vertical velocity W is the time rate of change of Δ of a fluid particle, so that

$$W = \left(U_r\frac{\partial}{\partial r} + \frac{U_\theta}{r}\frac{\partial}{\partial\theta}\right)\Delta(r,\theta). \tag{2.4}$$

Note that $W/U(h)$ is of $O[F^2 \times (\text{local slope})]$. The deflexion of a typical streamline Ψ_{H1} is shown in figure 2(*b*). Note that for all shapes of obstacles

$$\Delta(r,\theta) = W = 0$$

at the upwind stagnation line.

(*f*) Streamlines in [H_2], such as Ψ_{H2}, are not deflected.

† Note that $Fh = U/N$, so if α_B and α_T are independent of F, the thicknesses of [B] and [T] may be independent of the hill height h.

(*g*) As a consequence of the result (*b*), streamlines such as Ψ_T in figure 2(*b*) pass through region T and therefore over the top if they originate upstream at a height

$$H_s > h(1-\alpha_T F). \tag{2.5a}$$

In our experiment we shall test the hypothesis that $\alpha_T = 1{\cdot}0$, so that

$$H_s > h(1-F). \tag{2.5b}$$

2.2. *Lee waves and separation*

When the Froude number is of order unity then $h \sim U/N$; in other words, the length of waves (e.g. lee waves) set up in the stratified flow by the hill are of the same order as the height of the hill and they can then begin to control the flow (see figure 3). For a recent discussion of inviscid stratified flow over two-dimensional obstacles see Long (1972).

Either an asymptotic (Brighton 1977) or an order-of-magnitude analysis of stratified flow over two-dimensional hills with low or moderate slopes shows that the character of the surface boundary-layer flow depends primarily on the ratio of the wavelength of the lee waves ($2\pi U/N$) to the total *length* ($2L_0$) of the hill, rather than the height. For weak stratification streamlines and isopycnals are deflected by the hill by a distance of order h (i.e. h is characteristic of the amplitude of the waves) up to a height above the hill of the order of $2L_0$ (rather than h), producing a change in potential energy of the order of $-ghL_0\,\partial\rho/\partial z$; the change in kinetic energy is of order $\rho U^2(h/L_0)$, and so the dimensionless ratio determining the flow must be $(U/(L_0N))$. This ratio is proportional to the wavelength of a lee wave ($2\pi U/N$) divided by the length of the hill L_0. (For strongly stratified flow a different order-of-magnitude argument based on wave motion is needed.)

Some general conclusions about the way this ratio determines the flow can be drawn from the recent analytical and experimental work of Brighton (1977), the computational work of Sykes (1978) on laminar flow over two-dimensional hills, and the general observations of Scorer (1968). It appears that, when the stratification is such that $2\pi U/N \simeq 2L_0$, the region of flow separation in the lee of the hill is reduced to its minimum. For sufficiently steeply sided hills (e.g. a hemisphere) separation always occurs, but for flow over hills of moderate slope (e.g. less than 45°) separation can be totally suppressed. (For subsequent purposes this is our loose definition of moderate.) For all hills of moderate or steep slopes when the lengths $2L_0$ and $2\pi U/N$ differ considerably from each other, separation can occur in two different ways. If $2L_0 \gg 2\pi U/N$ (i.e. $F \ll 1$), separation is controlled by the pressure distribution produced by the lee-wave pattern, and, if $2L_0 \ll 2\pi U/N$ (i.e. $F \gg 1$), separation on the lee slope of the hill is controlled by the boundary-layer flow.

It is useful to designate the highest Froude number at which separation is first suppressed as the *critical Froude number for separation*, $F_{\mathrm{crit}(s)}$, and to describe flows for which F is greater than or less than $F_{\mathrm{crit}(s)}$ as super- or subcritical, respectively. (Normally these terms are used to denote the existence or non-existence of waves; hence the suffix s for separation.)

In practice any experiment has to be conducted in a flume or towing tank of finite depth D. In that case, the lee-wave pattern can be quite different, as may be seen in the case of two-dimensional hills by comparing the computed streamlines of Huppert

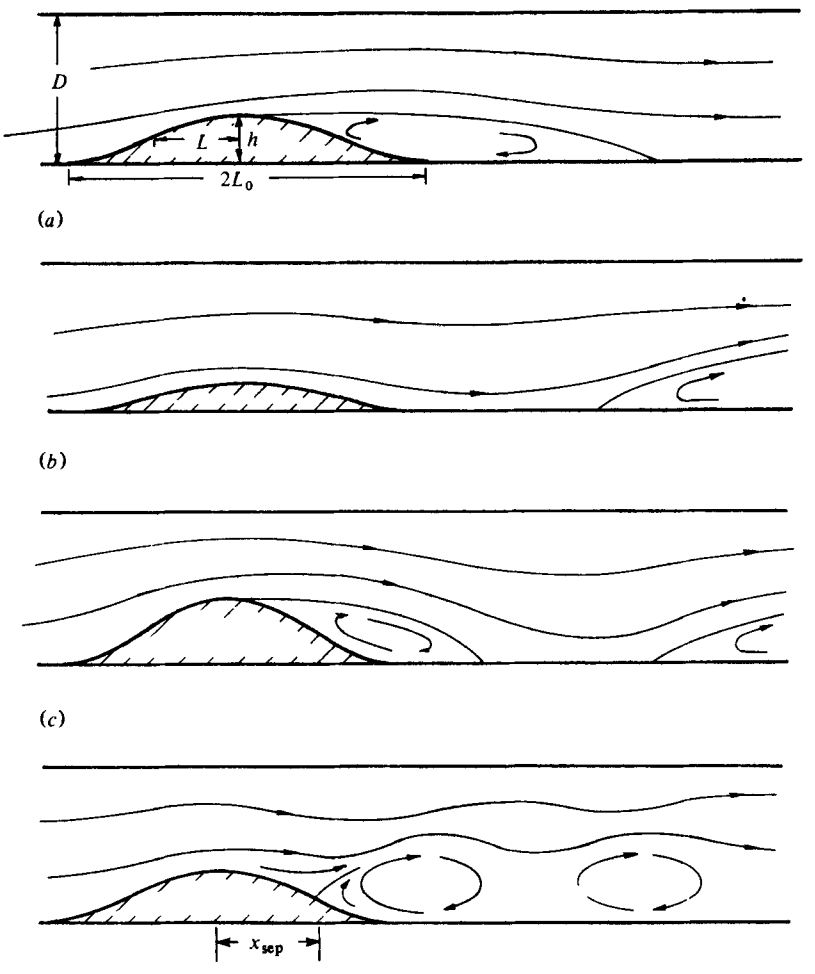

FIGURE 3. Stratified flow over two-dimensional hills in a channel. (*a*) Supercritical Froude number; no waves possible. $F_L > D/(L\pi)$ separation is boundary-layer controlled. (*b*) Hill with low slope; subcritical Froude number; no separation on lee slope; separation caused by lee wave rotor. $(1/\pi)\,(1-\pi^2F_L^2L^2/D^2)^{\frac{1}{2}} < F_L < D/(L\pi)$. (*c*) Hill with moderate slope; supercritical Froude number; boundary-layer separation on lee slope. $5/2\pi \lesssim F_L < D/(L\pi)$. (*d*) Subcritical Froude number; lee wave induced separation on lee slope. $F_L < (1/\pi)\,(1-\pi^2F_L^2L^2/D^2)^{\frac{1}{2}}$.

(1968) for a semicircular hill in an infinite fluid, and of Davis (1969) in a finite channel (or see Turner 1973, pp. 61–62). Brighton (1977) has shown theoretically how, for laminar flow over two-dimensional hills with low slopes, separation is determined by the Froude number based on the depth of the tank F_D, and the Froude number $F_L(> F_D)$ based on a suitable length L of the hill, such as the semi-length at the half-height. When $F_D < 1/\pi$ (i.e. $F_L < D/(L\pi)$), the hill triggers off standing internal waves which have a wavelength $\Lambda = (2\pi U/N)\,(1-F_D^2\pi^2)^{-\frac{1}{2}}$ and which produce separation under a rotor a distance of the order of Λ downstream of the hill. (See also Long 1955.) It appears from Brighton's analysis of flow over hills with *low slopes* that the down-slope acceleration produced by this internal wave effectively suppresses separation on

wedge, like shipwaves, as was thought at first (Queney *et al.* 1960), though lee waves like ship waves occur wherever there are strong variations of the density gradient (Crapper 1962, p. 603)];

(*c*) do not decrease significantly with height (z) above the hill, and

(*d*) can have a greater amplitude than those of a two-dimensional hill.

These results suggest the following:

(*a*) The lee waves created by a three-dimensional hill must be just as much affected by the depth of the flume or tank as those of a two-dimensional hill. But the side walls are not likely to have much effect, provided the width of the tank is somewhat greater than $2L_0$, which it must be to avoid the normal 'blockage' effects.

(*b*) We can estimate the streamwise wavelength, Λ, of three-dimensional waves in a tank of depth D (assuming $D \gg L$) by assuming the spanwise wavelength over an axisymmetric hill is about $2L$ and using the linearized wave equation [e.g. the Boussinesq form of equation (31) of Crapper (1959)] then

$$\Lambda \simeq \frac{2\pi U}{N}\left[\frac{1-(1+L^2/D^2)\,F_L^2/4}{1-F_L^2/4}\right]^{\frac{1}{2}} \simeq \frac{2\pi U}{N}, \tag{2.8a}$$

if $L \ll D$.

(*c*) Since lee waves over a three-dimensional hill are just as strong, they should be able to suppress separation just as much as they do over a two-dimensional hill.

(*d*) Assuming that the general criterion for the suppression of separation on the hill crest is also $\Lambda \simeq 2L_0 \simeq 5L$ for three-dimensional hills, then it follows from (2.7*c*) and (2.8*a*) that separation on the lee side of a hill with moderate slope will be suppressed over a range of $0 < x < x_{\text{sep}}$, when

$$\frac{x_{\text{sep}}}{\pi L} \lesssim F_L(1-F_L^2L^2/8D^2) \lesssim 0{\cdot}8. \tag{2.8b}$$

In discussing flows over two-dimensional and three-dimensional hills we have not compared the flows on the upwind side of the hills, because there is no real similarity. Two-dimensional flows exhibit the phenomenon of 'blocking' (see Turner 1973, p. 79) as the Froude number decreases, while in three-dimensional flows the effect of the hill only extends upwind a distance of order of the hill diameter.

There is an important constraint in deriving the flow pattern in stratified flows. If the diffusivity $\mathscr{D}$ of heat (if temperature stratified) or salt (as in our towing tank experiments) is small enough (i.e. $\mathscr{D}/(Uh) \ll 1$), if the turbulent mixing in the wake is weak, and if the velocity, pressure, and density distributions far downstream are the same as upstream, then fluid particles starting at a height z upstream must return to a height z downstream. This implies, where mean streamlines and mean particle paths (from points upwind of the hill) are close together (which is only true in weak turbulence), that no streamline starting at height $z > 0$ can be the streamline that attaches to the plane $z = 0$ at the downstream attachment point, as will become clearer in §4.

3. Apparatus

3.1. *Large towing tank experiments*

The experiments were conducted in both towing tanks and the wind tunnel of the EPA Fluid Modeling Facility. Details of the experimental apparatus are shown in

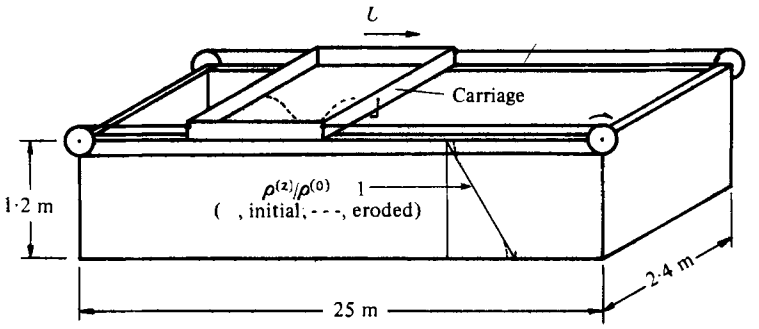

FIGURE 4. EPA water channel with towing carriage.

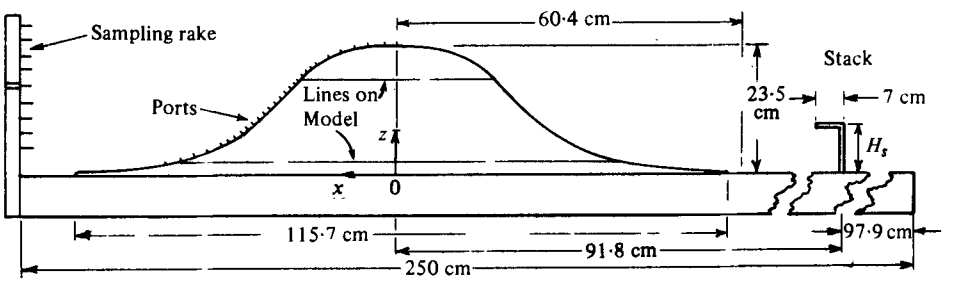

FIGURE 5. Details of polynomial hill model.

figures 4–7. The large towing tank is 1·2 m in depth, 2·4 m in width, and 25 m in length. It has an aluminium framework, and the sides and bottom are lined with acrylic plastic for viewing purposes. A towing carriage allows models to be towed the length of the tank at speeds from 5 to 50 cm s^{-1} (see figure 4 or for additional details Thompson & Snyder 1976 or HSL).

Coupled with the tank is a filling system (similar to that described by Pao *et al.* 1971) that allows the tank to be filled with an arbitrary stable density profile using salt water. Figure 4 shows one of the density profiles and compares it with another measured after 13 days and more than 15 tows of the hill through the tank. The initial profile is quite linear with a Brunt–Väisälä frequency of $N = 1{\cdot}33$ rad s^{-1}. The later profile shows only a slight erosion of the gradient near the surface, i.e. the top 8 cm of water is near neutral in stability, with the bulk of the water having the original stratification.

The model hill was made of acrylic plastic by vacuum moulding onto a wooden former. Ideally, the shape was to be the inverse of a fourth-order polynomial, but, owing to imperfect construction techniques, the final shape was closer to

$$f(r) = h\left(\frac{1{\cdot}04}{1+(r/L)^4} - \frac{0{\cdot}083}{1+[(r-r_1)/L_1]^2} - 0{\cdot}03\right), \tag{3.1}$$

where $h = L = 22{\cdot}9$ cm, $r_1 = 20{\cdot}3$ cm, and $L_1 = 7{\cdot}6$ cm. This equation describes the shape of the hill to within ± 2 mm. The maximum slope was about 1·0.

This hill was mounted on a flat base-plate, suspended from the carriage through jackscrews, and towed upside down across the water surface. The base-plate was immersed approximately 4 mm for each tow. Details of the model hill mounted on the base-plate are provided in figure 5. Twenty-eight sampling ports were fixed on the surface along each of the radial lines $\theta = 180°$, $-165°$, $-90°$ and 0°.

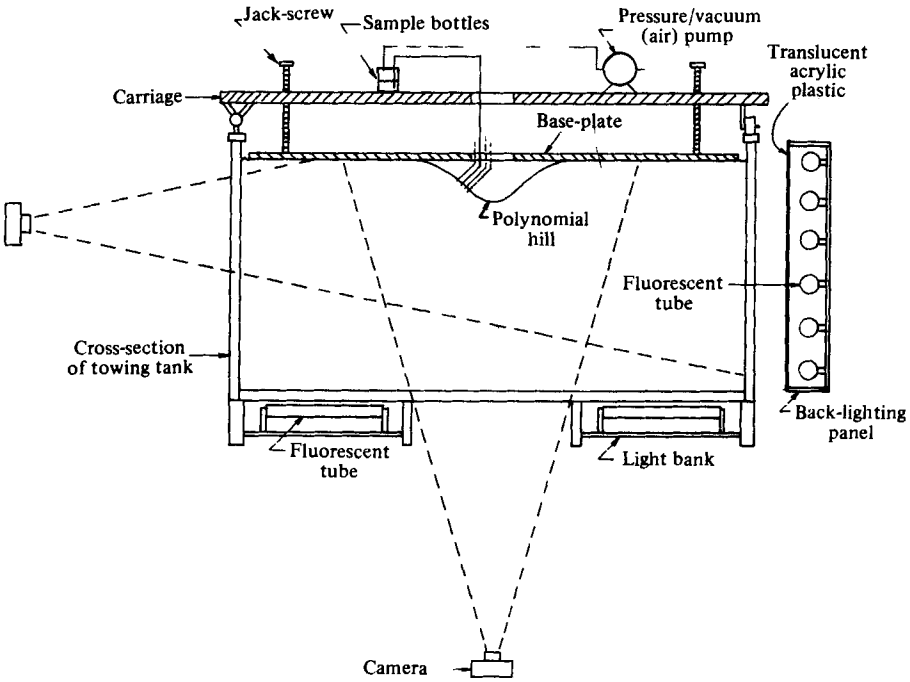

FIGURE 6. Detail showing suspension of model hill, lighting and photographic arrangement, and sampling and dye injection system in large towing tank.

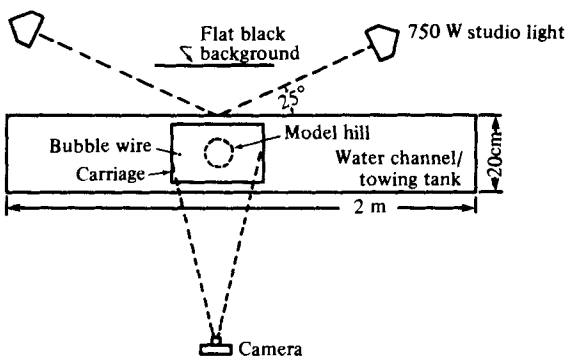

FIGURE 7. Plan view of set-up for photographing hydrogen bubbles in small towing tank.

The co-ordinate system is right-handed, with origin on the base-plate directly under the top centre of the hill. The positive x-axis points in the downstream direction and θ is measured from this axis.

As part of our study of the flow over the polynomial hill, dye was emitted isokinetically from a 'stack' of 0·635 cm o.d. The stack was bent through 90° parallel to the flow to avoid any cross-stream momentum in the effluent. It was located 91·8 cm ($4h$) upstream of the hill centre (see figure 5). The stack height H_s was varied from 0 to 1·2 hill heights. The effluent used was food dye diluted with the proper amount of salt water to obtain a neutrally buoyant plume, i.e. the density of the effluent was equal to the local density of the static fluid at the emission height of the stack.

In other tests, dye was released from the surface sampling ports on the windward and leeward hill centre-lines ($\theta = 180°$, 0°) to study the surface flow patterns, or alternatively through an injection rake emitting dye at 11 levels above ground at the stack position to study the centre-plane streamlines. To ensure that the dye solution at each port or tube would have the same density as the *static* fluid at the same height as the dye port with the hill stationary, salt solution was drawn through each port into small jars by application of vacuum pressure to a second tube fixed into the lid of the jars (see figure 6). Small amounts of concentrated dye were then added to each of the jars. Four different colours of dye were used in an alternating pattern for the surface ports to distinguish different levels. Then, with the carriage moving, the 'vacuum' tank was pressurized, forcing the dye and salt solution back through the ports into the flow around or upstream of the hill. Colour photographs and motion pictures were taken of the surface releases using this process at Froude numbers of 0·2, 0·4, 0·9, and 1·7. Black-and-white photographs of the upstream multilevel dye release were taken at Froude numbers of 0·2, 0·4, 1·0 and 1·7.

The multicoloured dye solution, the streamers from the upstream multilevel injection tubes, and the plumes from the upstream stacks were photographed from the side and from the bottom of the towing tank (the latter giving a top view of the hill). The photographic and lighting arrangements are also sketched in figure 6. Reflective lighting for the top views was provided by banks of fluorescent tubes placed just under the floor of the towing tank. The refraction of light by the salt solution resulted in some distortion and blurring, so that quantitative information was sometimes difficult to derive directly from the photographs.

Shadowgraphs were photographed using a 35 mm camera placed 9 m from a viewing screen of translucent drafting paper. The light source for the shadowgraphs was a lantern slide projector, placed 9 m from the model centre-line on the opposite side of the tank from the camera.

To obtain a better understanding of the surface flow patterns, granules of potassium permanganate were cemented to the hill surface. These granules dissolved rather slowly as the hill was towed through the tank, yielding bright purple streamers indicating the surface flow patterns. Because the streamers and the dye from the multilevel injection tubes were difficult to photograph at the higher tow speeds, the tank was filled with a much weaker stratification ($N \sim 0{\cdot}5$) so that surface flow and centre-plane streamline patterns could be photographed at high Froude numbers and low towing speeds. This provided an additional benefit in that it allowed an opportunity to observe the variation of the flow patterns with Reynolds number alone (see § 4.4).

One series of tests was run with the Froude numbers equal to 0·2, 0·4, 0·6, and 0·8 and stack heights equal to 0·2, 0·4, 0·6, and 0·8 hill heights in order to determine (*a*) whether the plume went over the hill or around it, (*b*) the impingement point z_i, defined as the height of the maximum concentration on the 180° line, and (*c*) the streamline deflexion at $\theta = -90°$. Samples were drawn during the tow simultaneously through all the surface ports using the sampling system described previously (figure 6). The collected sample jars were then visually inspected to determine which contained the highest concentration of dye.

The multilevel-dye-injection photographs were also analysed to obtain streamline deflexions over the top of the hill.

3.2. *Small towing tank experiments*

Some qualitative experiments were run in a small stratified towing tank 2·0 × 0·20 m and 0·10 m deep. The tank was filled by the usual 'two tank' method of Oster & Yamamoto (1963). Model hills were mounted on a base-plate suspended from a carriage similar in principle to that of the large tank. The hill used here had the same shape as the large hill; its height was 2 cm.

Shear-stress patterns were observed on the surfaces of several model mountains by a technique similar to the surface oil-flow technique commonly used in wind tunnel studies. The technique consisted of coating the models with a gelatinous solution of dye. The models were then clamped into place on the towing carriage and drawn through the tank. The dye was sheared away in regions of high stress and tended to collect along the stagnation areas, leaving a visual record of the surface flow patterns. This technique is, however, less satisfactory than the corresponding wind tunnel technique, because as the gelatin slowly dissolved, the dye separated from the surface with the flow at the separation points; these dye streaks, away from the surface, were superimposed on the surface flow patterns in the photographs.

A hydrogen-bubble-wire system (Schraub *et al.* 1965) was developed to study the streamline pattern and the velocity field on the centre-line of the hills. Time markers were produced by pulsing the voltage applied to the wires, generating distinct lines of bubbles. To generate bubble streaks, the wire was kinked by running it between two small gears (Clutter & Smith 1961). This provided a very uniform spacing of streaks, but was usable only at speeds in excess of about 8 cm s^{-1} because of problems with bubble rise.

The lighting and photographic arrangement used is shown in figure 7. Photographs were recorded with 35 mm camera equipped with 135 mm lens to reduce distortion due to parallax. Velocities were obtained from the photographs by determining the distance between successive bubble streaks.

3.3. *Wind tunnel experiments*

The identical polynomial hill was also used in the wind tunnel for flow studies under neutral stability conditions. The EPA Meteorological Wind Tunnel (Snyder 1979) has a test section 3·7 m wide, 2·1 m high and 18·3 m long. The air speed in the test section may be varied from 0·5 to 10 m s^{-1}. The hill was placed such that its apex was 424 cm from the entrance to the test section downwind of the contraction.

Turbulence measurements were made with Thermo-Systems Model 1054A anemometers in conjunction with Model 1243–20 cross film probes. The output signals from the anemometers were digitized at the rate of 1000 samples per second and linearized and processed on a PDP 11/40 minicomputer. Sampling (averaging) times of 1 min were found to yield reasonably repeatable results at the mean flow speed of 3 m s^{-1}.

One phase of the study involved visualization of smoke emitted from the stack upstream of the hill. Plume centre-lines were traced from photographs at various stack heights in order to obtain an idea of the centre-line stream-line pattern over the hill. Photographs were also taken of the smoke being emitted at low speed through the surface sampling ports to obtain an idea of the surface flow pattern.

4. Presentation and discussion of results

4.1. *Presentation of results*

Figures 8–13 present the visualization photographs. Figure 8 (plates 1 and 2) shows the flow patterns observed from the injection of multicoloured dye through the surface ports; figure 9 (plate 3) shows the surface shear-stress patterns observed from the gelatin-dye solution in the small towing tank and from the potassium permanganate granules in both the large and small tanks. The shadowgraphs of figure 10 (plate 4) show the change in the location of the separation point downstream of the hill as the Froude number changes. Figure 11 shows the streamers from the multilevel injection tubes upstream of the hill and tracings of smoke plume centre-lines from the wind tunnel tests. The speed-up over the top of the hill and the downstream lee-wave patterns are illustrated in the hydrogen-bubble photographs of figure 12. Figure 13 shows how plumes from upwind stacks impinge on the hill surface and/or go round the hill, depending on the Froude number.

Figure 14 presents the quantitative measurements of the flow structure with and without the hill in the wind tunnel. We have attempted to collate all the observations by drawing the surface shear-stress patterns and the mean centre-line streamline patterns for a number of different Froude numbers in figure 15. The classification of the surface singular points, denoted by P_i, are tabulated in table 1.

The plume impingement height is plotted as a function of the source height, and the hypothesis, $F = 1 - H_s/h$, is shown to be valid in figure 16. A streamline pattern over Elk Mountain, Wyoming, is presented in figure 17 for a rough comparison with the present observations. Figure 18 shows the displacement of streamlines above the hill top as a function of Froude number.

4.2. *Qualitative description of the flow*

At the lowest Froude number ($F = 0{\cdot}2$, figures 8*a*, *b*, *c*, 11*a*, 13*a* and 15*a*), the flow is, in large measure, constrained to move in horizontal planes. In a narrow region near the top of the hill, the flow has enough kinetic energy to overcome the potential energy and, thus, to go over the top. In the middle region, $[H_1]$ of figure 2, the plume rises slightly before it impacts on the surface, dips slightly from its upstream elevation as it goes round the sides, then rises again as it separates from the surface of the hill. Separation occurs as the flow goes round the sides at an angle of approximately 110° from the upstream stagnation line. A slight hydraulic jump occurs just downstream of the top of the hill, where Brighton's experiments at lower Reynolds number and lower Froude number indicated a 'cow horn' eddy with horizontal vorticity. The surface shear-stress patterns show a symmetric pair of more or less vertically oriented vortices downstream causing an upstream flow on the centre-line. The downstream dye release, however, shows the surface flow to be primarily perpendicular to the free-stream flow direction and to oscillate from one side to the other, broadly filling the wake with dye. There is only a very weak upslope component to the flow on the lower part of the lee-ward slope. Frequently, different colours of dye, emanating from different elevations on the surface, would be observed flowing in opposite directions (figure 8*c*). This oscillation of the flow in the wake also caused the plumes upstream of the hill to oscillate from side to side at low frequency (see, for example, figure 11*a*, at a lower Froude

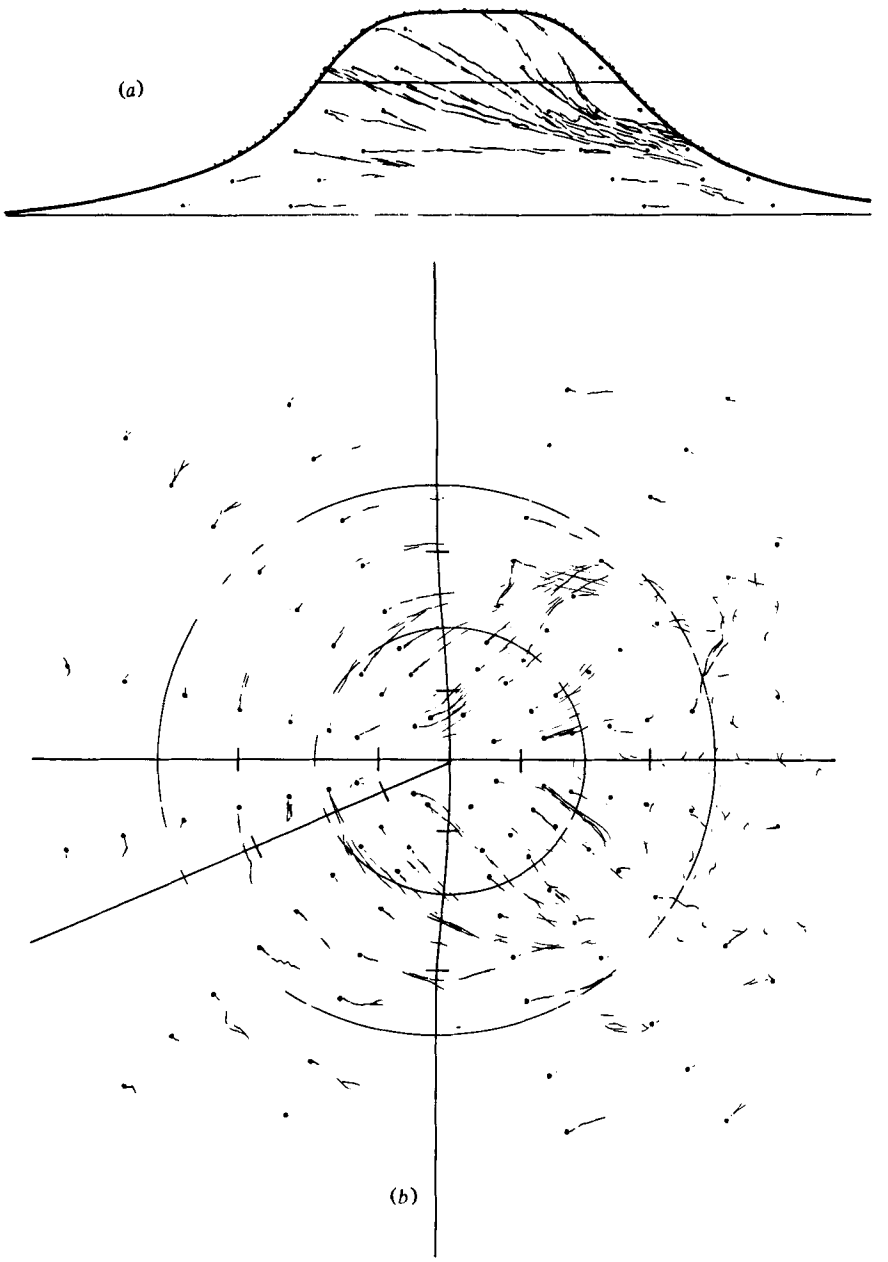

FIGURE 9. Visualization of surface shear stress patterns. (*a*) Side view of $KMnO_4$ streamers in large tank, $F = 0{\cdot}4$, $Re = 10000$. (*b*) Top view of $KMnO_4$ streamers in large tank, $F = 0{\cdot}4$, $Re = 10000$. See plate 3 for (*c*, *d*, *e*).

number of 0·1). A time sequence of photographs showed the plume (from a stack of height $H_s = 0{\cdot}4h$) oscillation to be irregular in amplitude and frequency. The lateral displacement of the plume impingement point reached as far as one-third the local hill radius on each side of the centre-line at a Froude number of 0·1. There was a significant component of energy at a vortex-shedding period of 33 s (which gives a local Strouhal

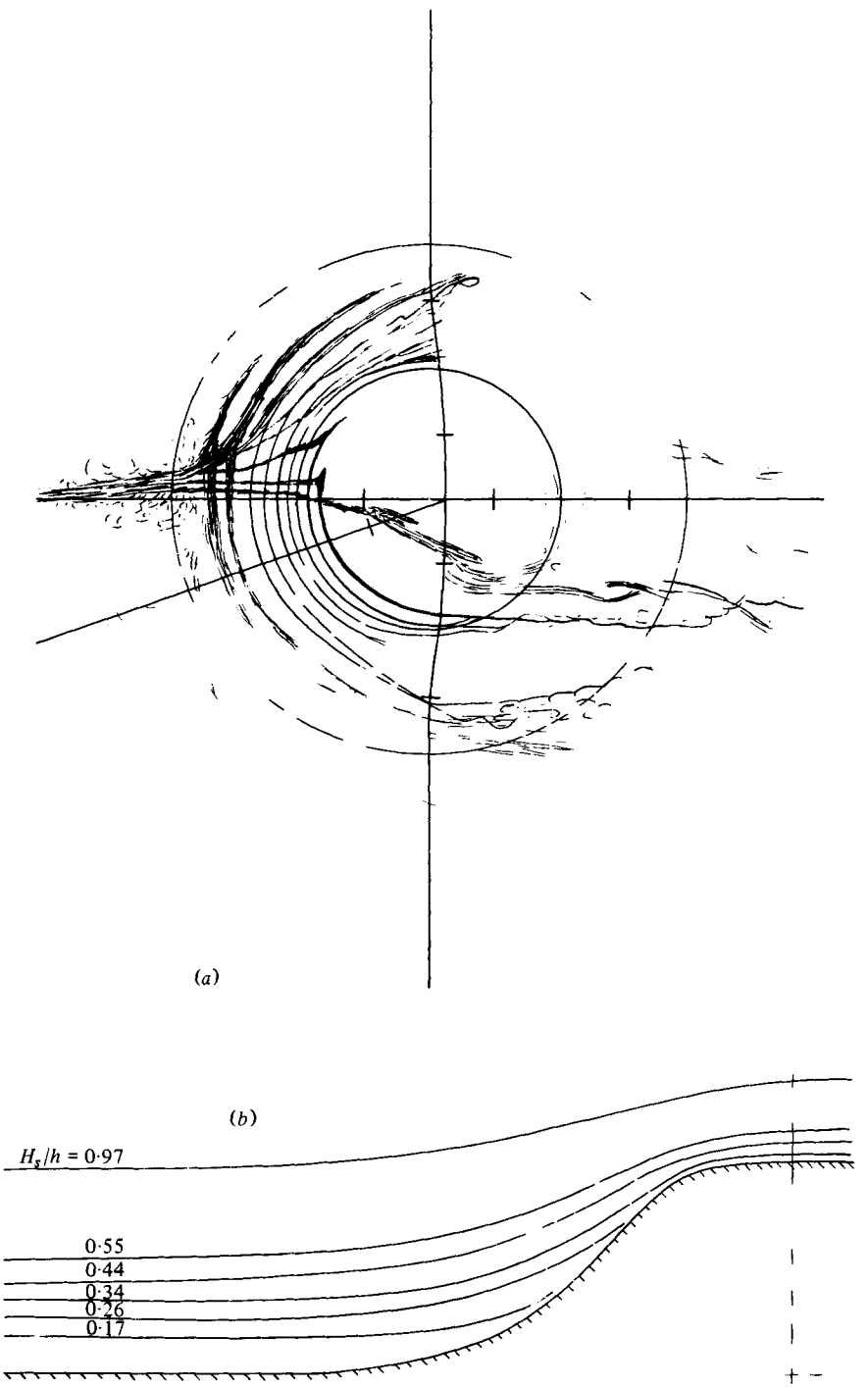

FIGURE 11. Experimental observations of centre-plane streamlines from multi-level tracer injection. (*a*) Instantaneous top view in large tank, $F = 0{\cdot}1$, $Re = 6900$. (*b*) Tracings of mean smoke plume centre-lines in wind tunnel, $F = \infty$, $Re = 45\,800$.

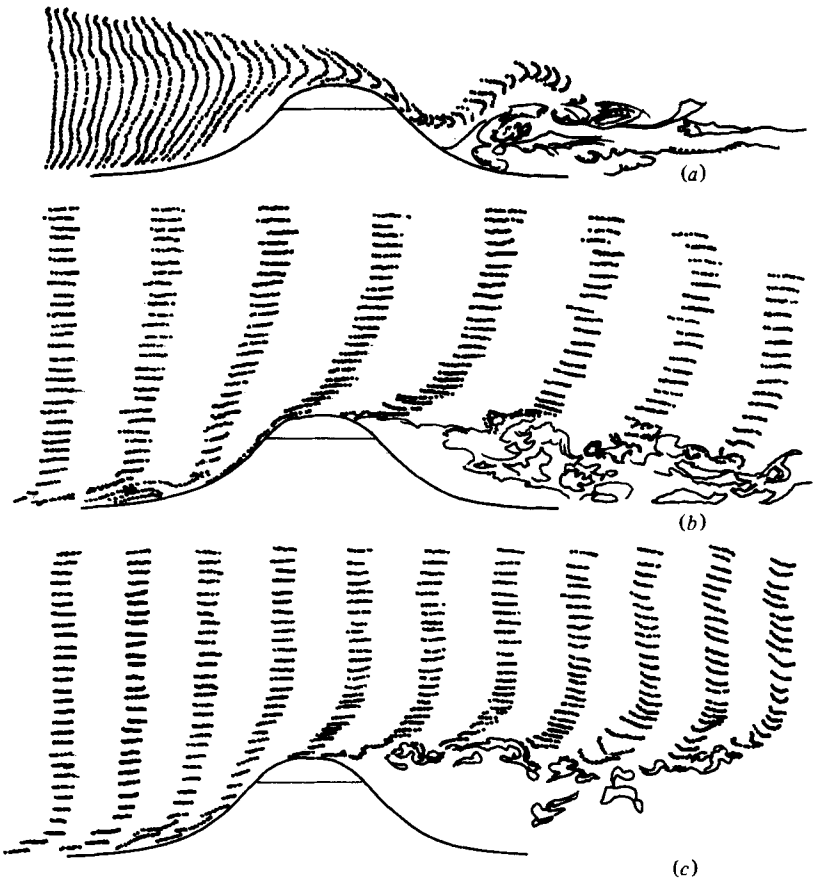

FIGURE 12. Sketches from Hydrogen-bubble photographs indicating speed-up over top of hill and the downwind lee wave pattern. (*a*) $F = 0{\cdot}4$, $Re = 1900$. (*b*) $F = 1{\cdot}7$, $Re = 3000$. (*c*) $F = \infty$, $Re = 1900$.

number $\cong 0{\cdot}5$ using the hill radius at the height of the stack), but, since this period differs with elevation and since the flows at different levels are not disconnected, some overall, apparently irregular, oscillation occurs (cf. Brighton, 1978).

A weak downslope flow on the windward centre-line results in a weak, perhaps intermittent, horseshoe vortex; its location appears to move up and down the slope. Indeed, the streamers from the upstream multilevel injection tube could be seen rolling up in vortices having one sign of circulation at one instant and the opposite sign at the next. Because of the problems with bubble rise, the hydrogen-bubble technique did not yield satisfactory results at this low Froude number.

At a Froude number of 0·4 (figures 8*d*, 9*a*, *b*, *c*, 12*a*, 13*b* and 15*b*), the flow has more energy to move in the vertical direction. The region where the flow goes over the top is now broader. At a stack height of only $0{\cdot}6h$, the plume is spread thinly to cover the entire upper half of the hill (figure 13). In the middle region [H_1], as at the smaller Froude number, the plumes rise somewhat before they impact on the hill; they dip significantly, however, from their upstream elevation as they go round the sides and continue losing elevation, at least for some distance downstream. In going round the sides, the flow separates from the surface at about the same point as it did at the

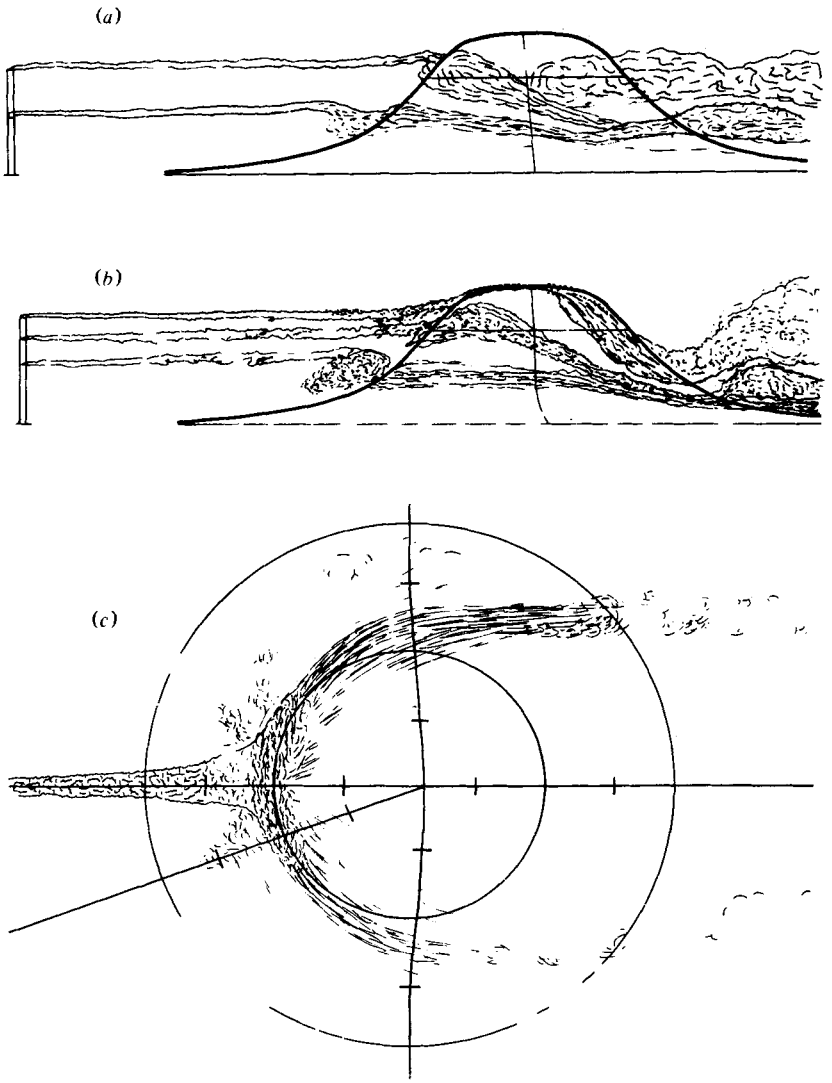

FIGURE 13. Plumes from upwind stacks at various elevations and Froude numbers in large tank. (*a*) Side view, $F = 0{\cdot}2$, $H_s/h = 0{\cdot}4$, $0{\cdot}8$, $Re = 13\,700$. (*b*) Side view, $F = 0{\cdot}4$, $H_s/h = 0{\cdot}4$, $0{\cdot}6$, $0{\cdot}8$, $Re = 27\,500$. (*c*) Top view, $F = 0{\cdot}6$, $H_s/h = 0{\cdot}4$, $Re = 41\,200$.

smaller Froude number (110°). In going over the top, however, the flow does not separate until it is roughly half-way down the lee slope. The shadowgraphs showed a strong hydraulic jump just downstream of this separation point. The height of this disturbance varied from 1·2 to 1·8 hill heights. The hydrogen-bubble photographs from the small towing tank show a weaker hydraulic jump but illustrate the lee wave pattern more vividly.

The surface shear-stress patterns again show a symmetric pair of vertically orientated vortices downstream causing an upstream flow on the centre-line. These vortices, however, are smaller and closer to the base of the hill (rather than farther downstream). Dye release from the downstream ports again showed the surface flow to be perpen-

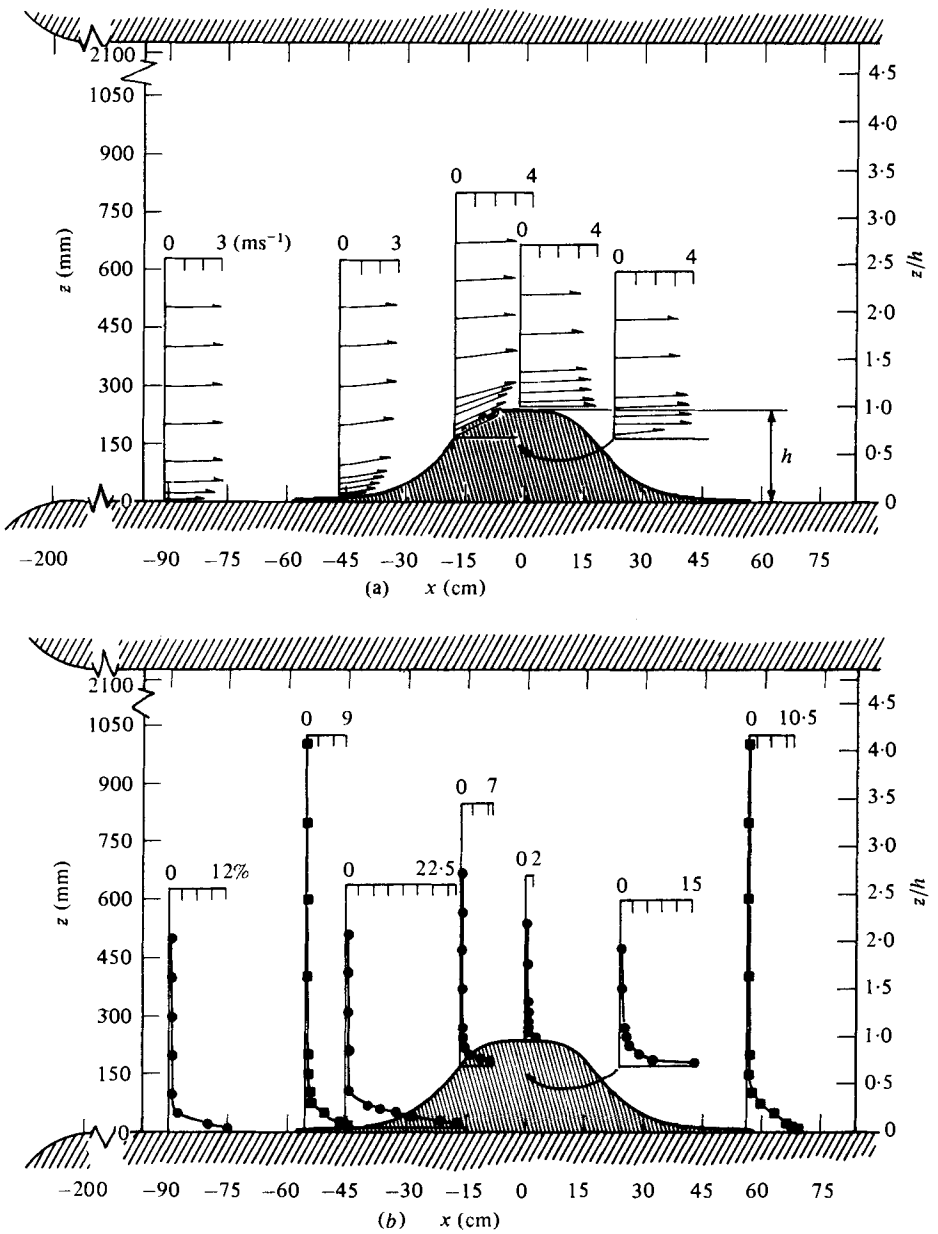

FIGURE 14. Wind tunnel measurements of the flow over and in the absence of the hill. (*a*) Mean velocity vectors (over the hill only). (*b*) Local longitudinal turbulence intensity profiles: ●, hill in place; ■, without hill.

dicular to the free-stream flow direction, to oscillate from side to side, and to broadly fill the (now narrower) wake. The motion picture film showed this more clearly.

The reverse flow *down* the *windward* slope is much more prominent, with the plume from any stack less than $\frac{1}{2}h$ being rolled up into an intermittent horseshoe vortex. At a stack height of $0{\cdot}2h$, the location of the point of maximum concentration was *lower* in elevation than at the lower Froude number of 0·2.

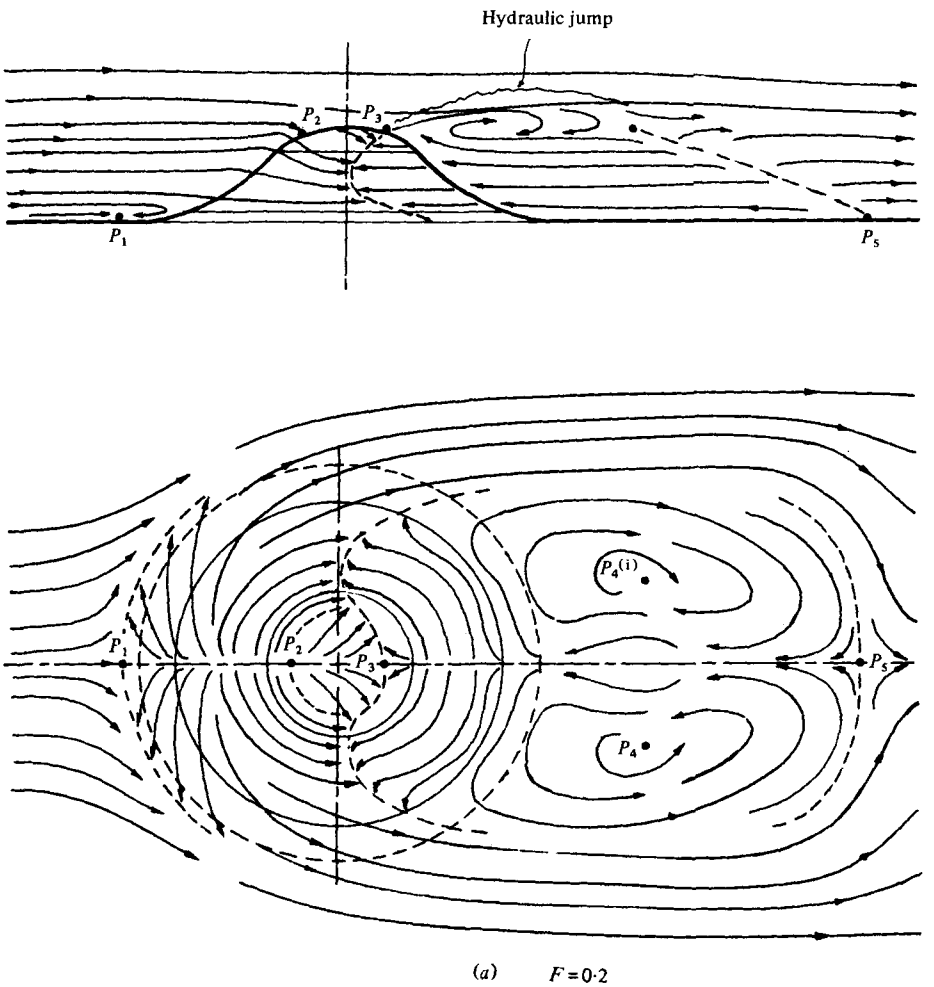

FIGURE 15. Derived centre-plane streamline and surface shear-stress patterns.

At a Froude number of 0·6, separation begins near the downwind base of the hill and the hydraulic jump peaks approximately two hill heights downstream of the hill centre (see figure 10*a*). At a Froude number of 0·8, separation began even farther downstream and the hydraulic jump peaked somewhere beyond three hill-heights downstream.

At a Froude number of 0·9 (figure 8*e*), all the flow in the centre-plane goes over the top of the hill, but a plume starting at ground level, on the centre-line and upstream of the hill would be spread out and would cover nearly the entire hill surface. The flow goes down the leeward slope without separating. At a slightly higher Froude number (1·0), a hydrogen-bubble photograph and the surface shear-stress patterns (figure 9*d*) clearly showed separation at the top of the lee slope. However, neither the streamers from the multilevel injection tubes nor the shadowgraph (figure 10) made this separation bubble visible. Evidently, the flow is on the *verge* of separating from the top of the lee side of the hill; the existence or non-existence as well as the size of the recirculating

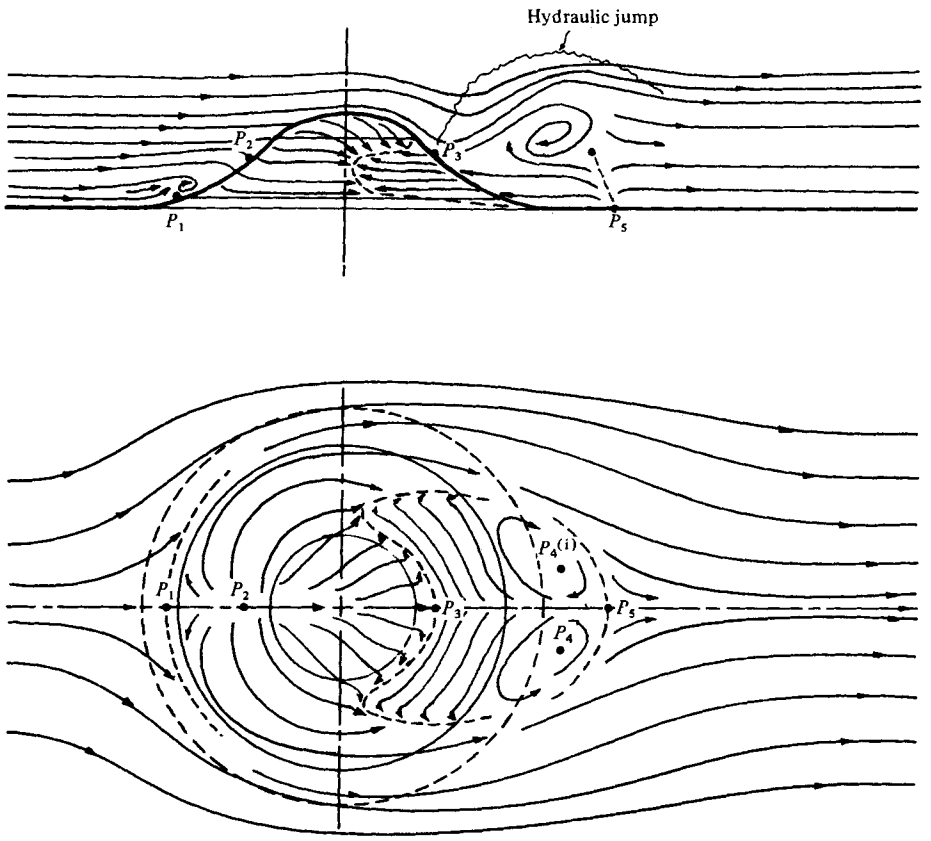

(*b*) $F = 0{\cdot}4$

FIGURE 15. For legend see p. 690.

region is evidently critically dependent on the exact Froude number, the Reynolds number, and the precise upstream flow conditions (figure 15*c*).

As the Froude number is increased further, the size of the recirculating region grows and the wake dimensions grow laterally and vertically. At a Froude number of 1·7 (figures 8*f* and 15*d*), the flow separates just past the top of the hill, resulting in a large recirculating region on the leeward slope. Again, a plume starting at ground level on the upstream centre-line would spread thinly over the entire hill surface. This flow resembles neutral flow except that the streamlines are closer to the top of the hill and they lose elevation much faster in the wake of the hill, as the large-scale lee wave streamline pattern descends to the ground (in this case $\Lambda \simeq 10L$).

Smoke visualization in the wind tunnel ($F = \infty$) showed the plumes to be spread thinly over the entire hill surface. Observing smoke released from the surface ports on the upwind face showed that the flow speed was low on the lower half of the slope and fairly high on the upper half. The release from the downwind ports showed the flow to be up the slope, separating upstream of the hill centre. Large fluctuations in the flow field were evident; for example, the horseshoe vortex *may* exist intermittently low

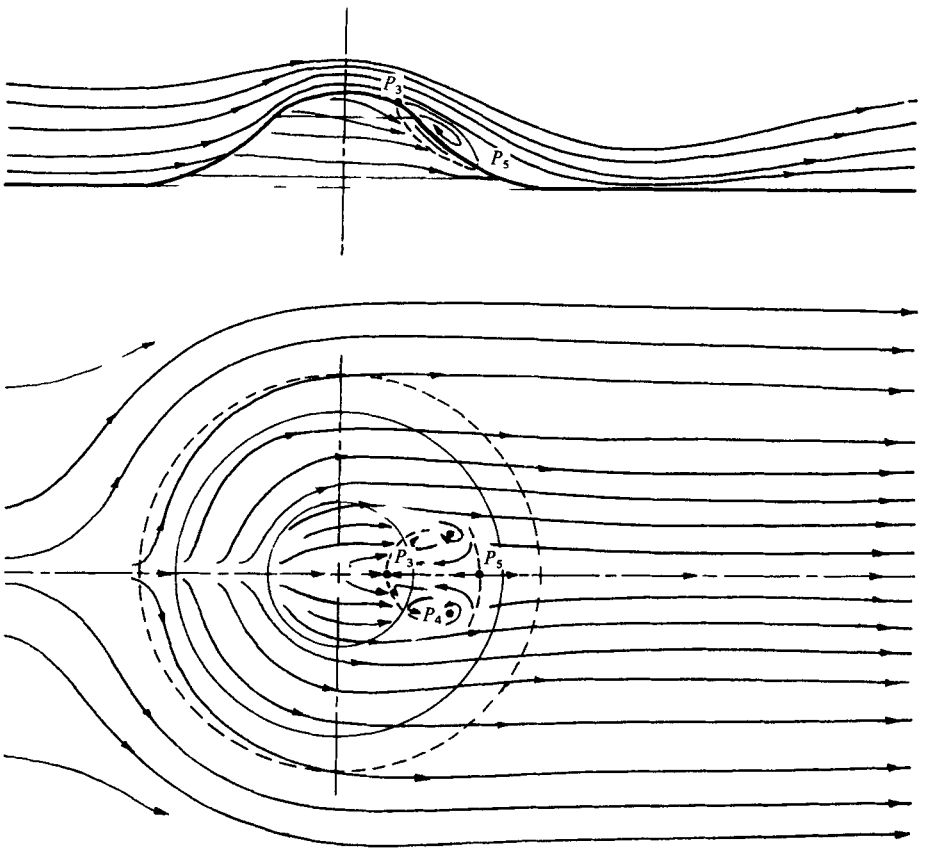

(*c*) $F = 1{\cdot}0$

FIGURE 15. For legend see p. 690.

down on the upwind slope. But the up-slope flow pattern and the separation position at the top front were fairly steady.

Measurements of the velocity fields with and without the hill in place in the wind tunnel ($F \simeq \infty$) are presented in figure 14; we have only included the mean velocity vectors and local longitudinal turbulence intensity profiles [for other profiles see HSL]. Vertical turbulence was measured and was found to be about half the longitudinal component everywhere. The free-stream speed U was 3 m s^{-1}. From the graphs, it may be seen that the boundary layer over the smooth tunnel floor was approximately 65 mm thick at the centre of the hill (but in the absence of it). The free-stream turbulence intensity was typically less than 0·5 %. The filling out of the velocity profiles on the upwind slope of the hill and the overspeed regions on the top and side are evident.

The mean velocity vectors show quite significant vertical components as far as two hill-heights upstream and up to twice as high as the hill itself. Directly above the hill and on the side, however, the vertical components are essentially zero. The abnormally high turbulence intensities at the upwind base of the hill are most likely caused by the abrupt step (6 mm) from the wind tunnel floor to the hill only a short distance upstream

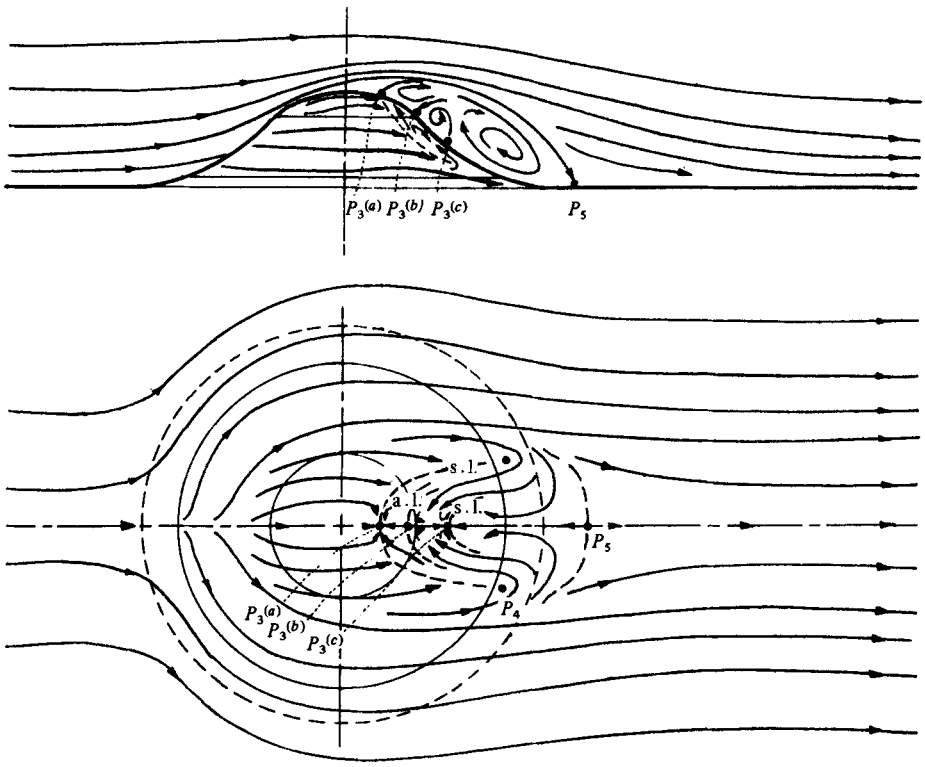

(*d*) $F = 1{\cdot}7$

FIGURE 15. For legend see p. 690.

from there. The very small turbulence intensities observed on the top and side of the hill are a result of the extremely thin boundary layers at those points, caused by the speed-up.

4.3. *Comparison with theory*

From all the observations at low Froude number ($F < 0{\cdot}4$), we can see the validity of the theoretical description of the flow (given in §2) for the asymptotic region [H_1]. That is, the velocities are primarily horizontal and the impinging streamlines are deflected downwards (unlike neutral flow where they mainly move upwards).

Unlike the smaller scale experiments of Brighton (1978), where the flow was everywhere laminar, a most important feature of these experiments is that the boundary layer on the surface of the hill is turbulent. Despite this, the low Froude number theory is approximately valid. This gives additional support to the validity of this scaling to the atmosphere, where almost always the surface flow is turbulent.

Of great practical importance is the height z_i at which the plume impinges on the hill. The asymptotic theory when $F \ll 1$ predicts that, when $H_s < h$, $z_i = H_s$ (equation 2.5). The values of z_i/h are plotted against Froude number in figure 16 for various values of H_s/h. The latter figure and figures 11 and 13 show rather convincingly, at least for this hill, that when $H_s > h(1-F)$ [our hypothesis: equation (2.5)], the plume touches the top of the hill or rises over it. Note that, if $h > H_s > h(1-F)$, the

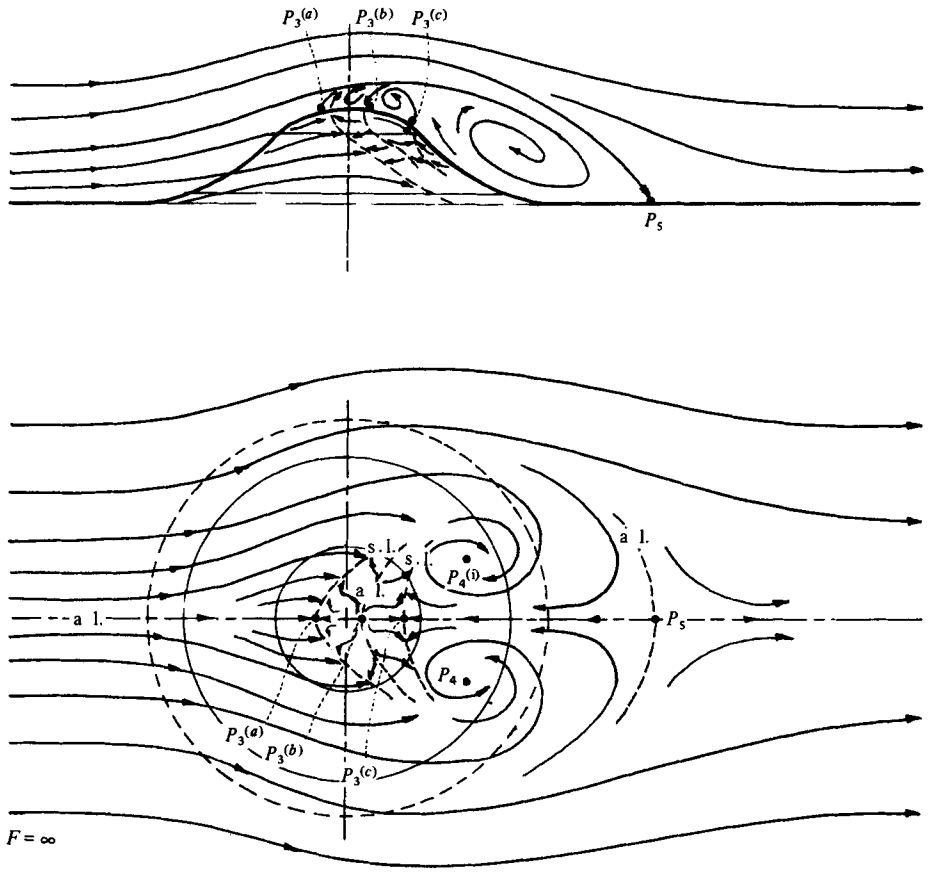

FIGURE 15. For legend see p. 690.

streamlines are observed to pass down the lee side of the hill very close to the surface, as if the top of the hill was a hill of height (Fh) on a plane at $z = h(1-F)$.

The photographs of surface dye releases also support the hypothesis that the summit region [T] has a thickness of Fh. Figures 8 (a) and (d) show that dye from the ports moves upwards rather than horizontally or downward when $z/h > 0{\cdot}82$ for $F = 0{\cdot}2$, and $z/h > 0{\cdot}61$ for $F = 0{\cdot}4$, compared with predicted values of 0·80 and 0·60.

The maximum observed downward deflexions at $\theta = 90°$ are compared in table 2 with values computed from (2.3) using potential flow theory and from (2.2) using a free-streamline model for U_θ, following Riley *et al.* (1976), which gives a maximum value for U_θ/U of about 1·4 when $\theta = 90°$. H_s is the upstream height of the observed streamlines.

When $F = 0{\cdot}2$, the observed vertical deflexion in the middle region, [H_1], is only slightly smaller than that calculated from (2.3), but about twice as large as that computed using the free-streamline model. The agreement is poor near the top of the hill in region [T] as was expected. When $F = 0{\cdot}4$, the deflexions calculated from (2.3) are greater than the upstream height of the streamlines, which is, of course, absurd; the theory is obviously invalid at this Froude number. The free-streamline theory overestimates the deflexions by a factor of two to three.

Froude no.	P_1 (x, y)	P_2 (x, y)	P_3 (x, y)	P_4 (x, y)	P_5 (x, y)
0·2	$\{S\}^{(s)}$ $(-2{\cdot}4, 0)$	$\{N\}^{(a)}$ $(-0{\cdot}4, 0)$	$\{S\}^{(s)}$ $(0{\cdot}4, 0)$	$\{N\}^{(s)}$ $(3{\cdot}4, -0{\cdot}9)$	$\{S\}^{(s)}$ $(5.8, 0)$
0·4	$\{S\}^{(s)}$ $(-1{\cdot}8, 0)$	$\{N\}^{(a)}$ $(-1{\cdot}0, 0)$	$\{S\}^{(s)}$ $(1{\cdot}0, 0)$	$\{N\}^{(s)}$ $(2{\cdot}4, -0{\cdot}5)$	$\{S\}^{(s)}$ $(3, 0)$
1·0			$\{S\}^{(s)}$ $(0{\cdot}5, 0)$	$\{N\}^{(s)}$ $(1{\cdot}2, -0{\cdot}4)$	$\{S\}^{(a)}$ $(1{\cdot}6, 0)$
1·7			$\{S\}^{(s)}$ $(0{\cdot}4, 0)$ $\{N\}^{(a)}$ $(0{\cdot}8, 0)$ $\{S\}^{(s)}$ $(1{\cdot}2, 0)$	$\{N\}^{(s)}$ $(1{\cdot}8, -0{\cdot}7)$	$\{S\}^{(a)}$ $(3{\cdot}4, 0)$
∞			$\{S\}^{(s)}$ $(-0{\cdot}3, 0)$ $\{N\}^{(a)}$ $(0{\cdot}2, 0)$ $\{S\}^{(s)}$ $(0{\cdot}6, 0)$	$\{N\}^{(s)}$ $(1{\cdot}3, -0{\cdot}7)$	$\{S\}^{(a)}$ $(3{\cdot}5, 0)$

Notes. (i) Singular points denoted by P_i are shown in figure 15. (ii) $\{S\}$ are saddle points; $\{N\}$ are node points in the pattern of surface-shear-stress lines; $\{\}^{(a)}$ are attachment points; $\{\}^{(s)}$ are separation points. (iii) Co-ordinates of P_i are given relative to the centre of the hill and are normalized in terms of the hill height, h. (iv) The singular points P_3 may, in fact, be three singular points as found at $F = 1{\cdot}7$ and $F = \infty$ (see figure 15*e*).

TABLE 1. Classification and location of singular points on polynomial hill.

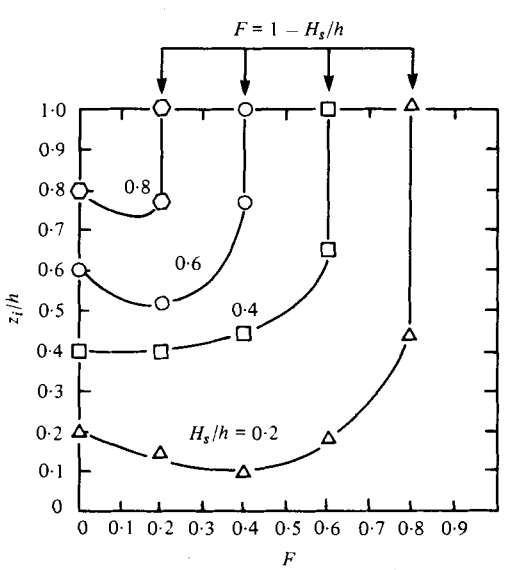

FIGURE 16. Height of plume impingement on the hill surface. [Note comparison with the hypothesis $F = 1 - H_s/h$ of equation (2.5*b*).] △, $H_s/h = 0{\cdot}2$; □, $H_s/h = 0{\cdot}4$; ○, $H_s/h = 0{\cdot}6$; ⬡, $H_s/h = 0{\cdot}8$.

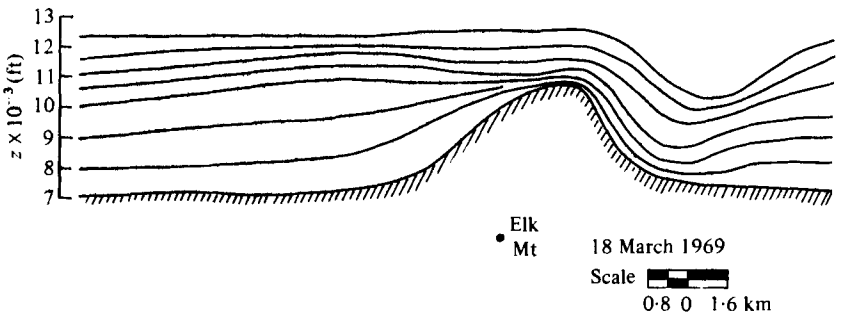

FIGURE 17. Streamline distributions over Elk mountain, Wyoming, estimated from aircraft observations (diagram taken from Kitabayashi, Orgill & Cermak 1971 and originally from Marwitz *et al.* 1969).

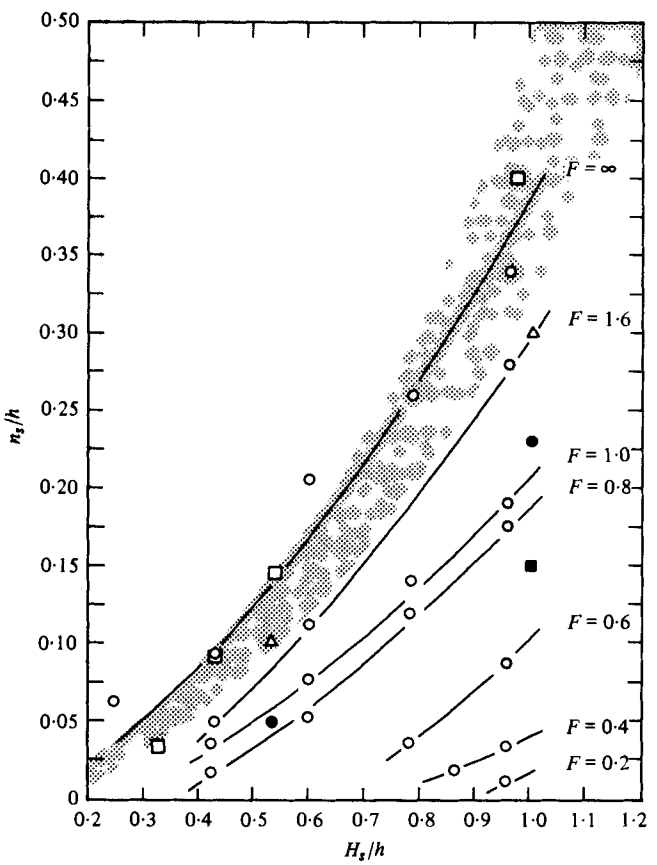

FIGURE 18. Displacement of streamlines above hill surface. Shaded area corresponds to potential flow theory for a range of *ellipsoids* where $h = b$ and $b \leqslant L_0 < \infty$: $\frac{1}{3}(H_s/h)^2 \lesssim n_s/h \lesssim \frac{1}{2}(H_s/h)^2$. ○, large tow tank; □, wind tunnel, $F = \infty$; ●, small tow tank, $F = 1·7$; ■, small tow tank, $F = 1·0$; △, small tow tank, $F = \infty$.

Froude number	H_s/h	$-\Delta/h$ at $\theta = 90°$ Observed	Calculated equation (2.3)	Calculated (free-streamline theory)
0·2	0·20	> 0·15	0·25	
0·2	0·40	0·12	0·17	0·08
0·2	0·55	0·16	0·16	0·08
0·2	0·60	0·21	0·17	
0·2	0·80	0·08	0·25	
0·4	0·40	0·12	0·67	0·32
0·4	0·55	0·10	0·64	0·32
0·4	0·60	0·38	0·67	

TABLE 2. Comparison of observed and calculated streamline deflexions.

Riley *et al.* (1976) and Brighton (1978) investigated the flow around model hills that did not slowly widen at their base; their hills all had gradients greater than or equal to one near the base. The flow pattern produced by this type of hill is quite different from one whose gradient tends to zero near its base (i.e. $dR_0/dz \to \infty$ as $z/h \to 0$). This slope tends to produce a large deflexion when $z/h < 0{\cdot}1$. This shape of hill also produces a downflow on the upstream centre-line of the hill, resulting in a large negative deflexion at $\theta = 180°$, whereas the theory predicts *zero* deflexion on the upstream stagnation line. This is part of the explanation for the vortex on the lower upstream side of the hill seen in figure 15(*a*). This vortex exists in the base region [B] (see figure 2*a*), where the asymptotic theory described in §2 is invalid. The vortex is necessary kinematically if the other singular point classification in figures 15(*a*) and (*b*) and table 1 are correct.

Another possible explanation for the differences between theory and experiment is that the plume diffuses downwards more than upwards when $z/h < \frac{1}{2}$ because Δ increases rapidly as z decreases when $z/h < \frac{1}{2}$. It may be erroneous to assume that the centre of the plume is the mean streamline through the source.

The surface shear stress lines and the mean centre-line streamlines are sketched in figure 15. It must be remembered when viewing these figures and comparing them with the various photographs that the photographs are *instantaneous* pictures. Whereas we have tried to pick representative ones, the details may vary markedly from the average conditions. The sketches represent our best judgment of the *mean* patterns. It was not possible, for example, to show the oscillation in the wake at low Froude number or the oscillation of the plumes on the upwind side in the sketches. (Typically at any one instant in the oscillation, there might be only *one* vortex on one side near P_4 and a single stagnation point near the point P_3.)

Figure 15(*a*) and (*b*) show some aspects of the complicated separated flow in the rear of a bluff three-dimensional hill when $F < 1$. The mainly horizontal motion around the hill region [H_1] induces a boundary-layer motion on the hill which separates, much as on a circular cylinder. The angle of separation is about 110° from the upstream stagnation line. This compares to about 80° for a circular cylinder at the same Reynolds number of 10^4, or since the surface flow is very turbulent, separation might occur at 100° or even 110°.

When $F = 0{\cdot}2$, figures 8(a) and 13 show that centre-line streamlines in region [H_1] starting upstream at a height $H_s(< h(1-F))$, rise suddenly on meeting the three-dimensional separation streamline surface. This surface intersects the hill surface on the critical shear stress line through P_3. These centre-line streamlines return approximately to their upstream level but also experience vertical mixing through a depth of about Δ. It would be misleading to describe this rise of the streamlines as a *jump*. However, the centre-plane streamline over the top of the hill does experience a sudden vertical rise and strong vertical mixing which can reasonably be called a local internal hydraulic jump. The plan view of the wake shows vigorous horizontal mixing through the wake.

When $F = 0{\cdot}4$, there is a strong downflow on the lee side which develops into a huge wave or hydraulic jump whose height varies from $1{\cdot}2h$ to $1{\cdot}8h$. This value is less than that found behind two-dimensional model hills (e.g. Davis 1969). Notice that the downstream wave or jump is highly curved and does not seem to extend laterally beyond the width of the hill. At lower Froude numbers, Brighton (1978) observed a curved trailing vortex rather than a jump.

As the Froude number is increased to about 1·0, the separated flow region is reduced even further in size (see figures 8e and 15c). Note that since there can be no mean particle paths that start at a finite height upstream and end on a ground level attachment point (§2.3), the streamline separating from P_3 probably reattaches at P_5. But since no surface streamline is observed to connect P_3 to P_5, the flow within the separated region is three-dimensional. At the nodal points, P_4, $P_4^{(i)}$, the surface flow swirls in, upwards, and eventually leaves downstream (figure 9d). Downwind of P_5 one or more lee waves develop. On the upstream side we observe that streamlines emanating from a height H_s above about $\frac{1}{2}h$ pass over the top, while those below that impinge onto the hill (the hypothesis of §2.1 for z_i is not valid when $F \geqslant 0{\cdot}5$).

The flow patterns shown in figures 8 and 11 not only indicate the path of the centre-line of the plume but also the mechanisms controlling the width of the plume. Over the hill the vertical plume width is reduced by the streamlines converging in the vertical plane, and the horizontal width is amplified by the divergence in the horizontal plane. There is also an indirect effect due to the density gradient being increased by the convergence of the streamlines in the vertical plane.

In figure 17 the streamline pattern over Elk Mountain, Wyoming, estimated from aircraft observations by Marwitz *et al.* (1969) is shown for comparison with figure 15. The density distribution was different from that in our tank, there being a well-mixed layer below a fairly sharp inversion, but the gross Richardson number ($\simeq F^{-\frac{1}{2}}$) was about 1·0. It is interesting that these observations indicate that if $H_s/h > \frac{1}{3}$ the streamlines pass over the hill top, as in our experiments; for a streamline starting at $H_s/h \sim 1{\cdot}0$, these observations indicate that the distance n_s from the hill top to the streamline is $0{\cdot}1h$ whereas we found $0{\cdot}2h$ (see figure 18). Although these are of the same order the difference is significant and is probably due to the different upstream density gradient. Long's (1955) laboratory towing-tank experiments also showed that the lee-wave pattern was insensitive to a small well-mixed layer near the ground. The surface streamline patterns shown in figures 15(c) and (d) are similar to those inferred by Connell (1976) from his aircraft observations.

The main difference between the flow at Froude number 1·7 and neutral flow ($F = \infty$) is the location of the separation point on the top of the hill $P_3^{(a)}$ (figures 15e and 9d, e).

When $F = 1{\cdot}7$, P_3 is slightly *downwind* of the centre, and, when $F = \infty$, P_3 is *upwind*. The character and location of the other singular points is approximately the same. Another difference is that the streamlines are closer to the top when $F = 1{\cdot}7$ (figure 18).

The mean velocity $u(z)$ and turbulence profiles over the hill in neutral flow measured in the wind tunnel are shown in figures 14 (a) and (b). Note particularly in figure 14 (a) that the speed-up factor S over the hill is the same on the top as on the side of the hill, as is found over the central plane of an ellipsoid (Milne-Thompson 1960, p. 518). Defining S on the top as $S = u(1{\cdot}03h)/U_\infty(h)$, we find $S = 1{\cdot}27$. To allow for the separated region in the lee of the hill, as a reference value we might compute S for an ellipsoid, with half-width b_0 and half-length L_0, elongated in the direction of the flow such that $h = b$, and $L_0/h \simeq \frac{3}{2}$; from Milne-Thompson's expression we find $S = 1{\cdot}28$, which suggests that the measured value is of the right order. The turbulence measurements indicate the thickness of the upwind boundary layer and how its thickness is reduced by the large negative pressure gradient over the hill. There is effectively very little turbulence outside the boundary layer.

Figure 18 shows the displacement of streamlines above the hill surface as a function of upwind streamline height, derived from the multilevel tracer injection photographs. The neutral-flow data from the towing tank and from the wind tunnel match fairly closely, for the smaller values of H_s/h, the streamline displacements predicted by potential flow theory for flow over an ellipsoid, of width $2b$ and length $2L_0$. The theory predicts that, if $H_s \ll h$, and if $h = b$ and $b \leqslant L_0 < \infty$, $\frac{1}{3}(H_s/h)^2 \lesssim n_s/h \lesssim \frac{1}{2}(H_s/h)^2$ (see HSL). It is also evident from figure 18 that, as the stratification increases, the streamlines become much more closely packed, with important implications for diffusion. The data from the small towing tank consistently show smaller displacements than those from the larger facilities; this may be due to problems with bubble rise (the model was towed upside-down) or it may be a Reynolds number effect (the small towing tank is $\frac{1}{12}$ the size of the large tank).

How do the experimental flow patterns compare with the speculative predictions of §2.2 about the lee waves and the existence and position of separation? We first examine the nature of the separated flows at the four primary Froude numbers of our tests, and classify these as sub- or supercritical, according to the nature of the separation. For sub-critical flows ($F_L < F_{\mathrm{crit}(s)}$) separation on the centre-line of the lee slope is located where the flow in the downstream lee wave rotor leaves the surface, primarily an inviscid mechanism. For supercritical flows ($F_L > F_{\mathrm{crit}(s)}$), separation on the centre-line is determined by the boundary-layer behaviour on the lee slope under the action of the pressure gradient outside the boundary layer, which may, of course, be affected by the lee waves. With regard to the location of separation in boundary-layer controlled supercritical flow, separation occurs near the position of maximum curvature (near the hill crest as a rule) whereas in subcritical flow the separation occurs where the lee wave leaves the hill surface. We conclude without any doubt that, when $F = 0{\cdot}2$ and $0{\cdot}4$, the separated flows are subcritical and when $F = 1{\cdot}0$ and $1{\cdot}7$ the flows are supercritical; though in the larger tank, when $F = 1{\cdot}0$, the separated flow region is very small, and the flow is only just supercritical.

To become more specific about the location of separation, we observed that, when $0{\cdot}6 \lesssim F_L \lesssim 0{\cdot}8$, separation occurred downstream of the hill, as defined by $x_{\mathrm{sep}} \gtrsim 3/2L$. The range of F_L predicted by (2.8) for this value of x_{sep} is $0{\cdot}5$ to $0{\cdot}8$. When separation occurs on the lee slope caused by the short wavelength lee waves, we observed that,

F_L	Theoretical (three-dimensional internal waves) $\Lambda/L = 2\pi F_L$	Measured (at about $z = 2h$ from figure 12)	Character of separated flow: Predicted [based on (2.8*b*)]	Character of separated flow: Observed
0·4	2·5	2·0 ± 0·5	Subcritical	Subcritical
1·0	6·3	6·0 ± 1·5	Supercritical	Supercritical

Note that: (*a*) in our experiments $F_L = F$ because $L = h$, and (*b*) the ratio of the hill height h to that of the tank D is about 0·2 (for the large or small tank), so that the wavelength of the internal waves, given by (2.8*b*), is about equal to that of waves in an infinite medium, i.e. $2\pi U/N$.

TABLE 3. Lee waves estimates and separated flow classification.

when $F_L \simeq 0{\cdot}4$, $x_{sep} \simeq 0{\cdot}9L$ and, when $F_L \simeq 0{\cdot}3$, $x_{sep} \simeq 0{\cdot}7L$. The predicted range of F_L from (2.8) for these two values of x_{sep} are 0·27 to 0·8 and 0·21 to 0·8 respectively. It appears that the prediction in (2.7) for the range of Froude numbers required to suppress separation for a given value of x_{sep} is slightly in *excess* of the observed range of F_L. Alternatively for given F_L, the maximum value of x_{sep} predicted by (2.8) is slightly too large (e.g. $0{\cdot}9L$ as compared with $0{\cdot}7L$ at $F_L = 0{\cdot}7$).

When F_L is very small the separation pattern is probably dominated by the horizontal flow, because the lee-waves' amplitude is very small. For example at $F = 0{\cdot}1$, 0·2, the observed amplitudes are about $0{\cdot}04h$ and $0{\cdot}1h$, which are about $\frac{1}{2}N/U$ or $\frac{1}{2}Fh$. Thus the lee waves, as expected, are confined within the $[T]$ layer.

We used the hydrogen-bubble photographs, some of which are shown in figure 12, to estimate the wavelength Λ of the lee waves, to compare these with the natural wavelengths of the internal waves in the stratified flow, and to note the value Λ/L as the separated flow changed from a subcritical to a supercritical character. We tabulate these parameters in table 3.

4.4. *Flow variations with Reynolds number*

Most of the runs were done in the large towing tank at a fixed stratification ($N \cong 1{\cdot}33$ rad/s) and, in order to increase the Froude number, the towing speed was increased; this resulted in a corresponding increase in the Reynolds number. Systematic studies to examine the influence of Reynolds number on the flow patterns around the hill were not conducted. However, some experiments were done in the large tank with a weaker stratification ($N \simeq 0{\cdot}5$ rad/s), and also in the small tank, thereby yielding information at the same Froude number, but different Reynolds numbers. For example, at $F = 0{\cdot}4$, we have Reynolds numbers of 400 and 1900 from the small tank, 10 000 from the large tank with weak stratification, and 27 500 from the large tank with strong stratification. In the large tank, no variation with Reynolds number was observed; allowing for differences in visualization techniques and for slight differences in the shape of the hill and the absence of the 'square flange' in the small tank, it is also safe to say that only slight variations of the flow patterns with Reynolds number were observed. Our conclusions on the flow patterns were thus more heavily weighted by the results from the large tank. Extrapolations of these results to the atmosphere, where the Reynolds number may be several orders of magnitude larger, is a much more serious question, and no apologies are offered. It has been shown by numerous authors that many of the

flow patterns observed in the atmosphere, in particular lee waves and hydraulic jumps, can be simulated at much smaller Reynolds numbers (even considerably smaller than in the current experiments) in the laboratory.

5. Conclusions

(1) A flow structure to describe stably stratified flow over three-dimensional hills was developed from physical scaling laws, some primitive analyses, and analogy with two-dimensional hills. The experiments broadly confirmed the general predictions about the flow structure, the important features of which are summarized below.

(*a*) When $F \ll 1$ (say $F < 0{\cdot}3$ for hills with moderate slope), the flow is approximately horizontal except in narrow regions at the top [T] and bottom [B] of the hill. These regions have thicknesses of about Fh, and streamlines starting in region [T] tend to pass over the top of the hill. A small lee wave or internal hydraulic jump may be found on the lee side of the hill in region [T]. Below region [T] the flow separates on the lee side of the hill, where a mainly horizontal recirculating flow is found. However, there is some vertical mixing caused by streamlines, deflected downwards by about hF^2 outside the wake, entering the wake and reverting to their original height.

(*b*) When F is of the order of 1 but not very much less than 1 (say $> 0{\cdot}3$), then it is less useful to think in terms of perturbations from the asymptotic state of $F \to 0$. Rather, it proves better to think in terms of the response of the flow over the hill to the wavelength Λ of the lee-wave pattern set up by the hill. For two-dimensional and three-dimensional hills which have moderate slopes (i.e. are large enough for the flow to separate in neutral flow), it appears that:

(i) when $\Lambda \lesssim 5L$ or $F_L \lesssim 0{\cdot}8$ separation at the top of a symmetric hill is suppressed (this value of F_L we have denoted by $F_{\mathrm{crit}(s)}$);

(ii) if the Froude number is further decreased the flow travels smoothly over the top but separates under a lee wave on the downstream side of a point $x = x_{\mathrm{sep}}$, where x_{sep} satisfies the inequality

$$x_{\mathrm{sep}} \lesssim \tfrac{1}{2}\Lambda \quad \text{or} \quad x_{\mathrm{sep}} \lesssim \pi F_L.$$

[These conclusions are based on the experiments described here, on our experiments with a 126° cone and a hemisphere to be described in a later publication,† on experiments over two-dimensional ridges by Brighton (1977) at a Reynolds number of 400, on experiments by Davis (1969), and on computations by Sykes (1978)].

(*c*) When F is not much greater than 1, say, of the order of 1·5 or greater, overall, but not in detail, the flow structure around the hill becomes broadly similar to that of neutral flow. But far downstream the stratification may have a strong effect, even when F is as large as 10.

(2) The potential effects of the stratification on a plume (streamline) from an upwind or downwind source are summarized below. The implications for surface concentrations are amplified in another paper (Hunt, Puttock & Snyder 1979).

(*a*) The stronger the stratification, the narrower will be the vertical width and the wider will be the horizontal width of the plume. If it starts below the hill top, yet goes over the top, it will pass very close to the hill surface and be further contracted in the vertical and expanded in the horizontal.

† Snyder, Britter & Hunt (1979).

(*b*) The criterion for determining whether the plume will impact on the hill surface and go round the sides or go over the top is, roughly, $H_s = h(1-F)$, where H_s is the dividing streamline height, h is the hill height, and F is the Froude number characterizing the stratification. If the plume height (upstream) is smaller than this streamline height, it will impact on the hill surface; otherwise, it will go over the top.

(*c*) In moderately stratified flow (say, $0{\cdot}4 < F < 1{\cdot}5$), if the plume height is larger than $h(1-F)$, but not much larger than $h(1+F)$, the plume can still pass down the lee side of the hill very close to the surface.

(*d*) Although no sources were placed downwind of the hill, it is evident from the mainly horizontal recirculation patterns observed there in strongly stratified flows ($F < 0{\cdot}3$) that a downwind plume below $h(1-F)$ would also impinge on the hill surface. For weaker stratifications, plumes could also be brought rapidly to the ground as a result of the lee waves (descending streamlines) and rotors induced by the hill.

(3) Since our experiments were all conducted in an approach flow without shear, the application of the results of modelling to the atmosphere has to be more than usually justified. Turbulent unstratified flows around bluff bodies all have much the same *structure* of separation regions, singular points, etc., for large variations in the approaching shear because the body's own wake flow has such a strong controlling effect (Hunt, Abell, Peterka & Woo 1978). The actual position of upstream vortices can be changed, but the structure of the wake flows are remarkably similar. Thus, we speculate that since in a strongly stratified flow ($F \ll 1$) the flow is somewhat 'decoupled' at different heights the effect of the upstream shear on the flow structure close to the hill is likely to be small. But, of course, quantitative results such as the coefficient α_T defining the thickness of the $[T]$ region, and plume impingement height z_i/h or the speed-up factor S will be considerably influenced; we do not even know yet whether they will be increased or decreased!

(4) A more fundamental limitation of our experiments may be the fact that they were conducted in finite depth tanks. The approximate argument of § 2.2 suggests that the effect of the finite depth on three-dimensional lee waves is not very marked. Investigation of the lee-wave pattern in the large tank may help elucidate this question. Experiments are certainly needed in stratified flows where the density gradient varies with depth, as it always does in the atmosphere; but we hope that the general ideas about the relation between the wavelengths of lee waves Λ and the horizontal length scale of the hill L may still be useful for estimating when, where, and what kind of separated flows will occur.

J. C. R. H. is grateful to his research student Dr P. W. M. Brighton and to Dr H. E. Huppert for teaching him something about stratified flow over obstacles and to Dr Paul Mason and Mr Ian Sykes of the Meterological Office (U.K.) for enlightening conversations about lee waves. We are grateful to Mr Roger Thompson and Mr Daniel Dolan for help with the photographs, and to Mr Robert Lawson, Mr Lewis Knight, Mr Leonard Marsh, and the late Mr Karl Kurfis for help with running the experiments. Financial support for J. C. R. H. was provided through an appointment as Visiting Associate Professor, Department of Geosciences, N.C. State University, through EPA Grant R804653.

REFERENCES

BRIGHTON, P. W. M. 1977 Boundary layer and stratified flow over obstacles. Ph.D. dissertation, University of Cambridge, England.

BRIGHTON, P. W. M. 1978 Strongly stratified flow past three-dimensional obstacles. *Quart. J. Roy. Met. Soc.* **104**, 289–307.

BURT, E. W. & SLATER, H. H. 1977 Evaluation of the valley model. *AMS-APCA Joint Conf. on Appl. of Air Poll. Meteorology, Salt Lake City, Utah.*

CLUTTER, D. W. & SMITH, A. M. O. 1961 Flow visualization by electrolysis of water. *Aerospace Engng* **20**, 24–27, 74–76.

CONNELL, J. R. 1976 Wind and turbulence in the planetary boundary layer around an isolated 3-D mountain as measured by a research aircraft. *Int. Conf. on Mountain Met. and Biomet., Interlaken, Switz.*

CRAPPER, G. D. 1959 A three-dimensional solution for waves in the lee of mountains. *J. Fluid Mech.* **6**, 51–76.

CRAPPER, G. D. 1962 Waves in the lee of a mountain with elliptical contours. *Phil. Trans. Roy. Soc.* A **254**, 601–623.

DAVIS, R. E. 1969 The two-dimensional flow of a fluid of variable density over an obstacle. *J. Fluid Mech.* **36**, 127–143.

DRAZIN, P. G. 1961 On the steady flow of a fluid of variable density past an obstacle. *Tellus* **8**, 239–251.

HUNT, J. C. R., ABELL, C. J., PETERKA, J. A. & WOO, H. 1978 Kinematical studies of the flows around free or surface mounted obstacles; applying topology to flow visualization. *J. Fluid Mech.* **86**, 179–200; corrigendum *J. Fluid Mech.* **95**, (1979), 796.

HUNT, J. C. R. & MULHEARN, P. J. 1973 Turbulent dispersion from sources near two-dimensional obstacles. *J. Fluid Mech.* **61**, 254–74.

HUNT, J. C. R., PUTTOCK, J. S. & SNYDER, W. H. 1979 Turbulent diffusion from a point source in stratified and neutral flows around a three-dimensional hill. Part I. Diffusion equation analysis. *Atmos. Environ.* **13**, 1227–1239.

HUNT, J. C. R., SNYDER, W. H. & LAWSON, R. E. 1978 Flow structure and turbulent diffusion around a three-dimensional hill: fluid modelling study on effects of stratification. Part I: flow structure. *U.S. EPA Env. Monitoring Ser. Rep.* EPA-600/4-78-041. Res. Tri. Pk., N.C.

HUPPERT, H. E. 1968 Appendix to paper by J. W. Miles. *J. Fluid Mech.* **33**, 803–814.

KITABAYASHI, K., ORGILL, M. M. & CERMAK, J. E. 1971 Laboratory simulation of airflow and atmospheric transport-dispersion over Elk Mountain, Wyoming. *Fluid Dyn. and Diff. Lab. Rep.* no. CER 70-71 KK-MMO-JEC-65, Colorado State University, Fort Collins.

LARRSON, L. 1954 Observation of lee waves in the Jamt Land Mountains, Sweden. *Tellus* **6**, 124–138.

LIU, H. T. & LIN, J. T. 1975 Laboratory simulation of plume dispersion from lead smelter in Glover, Missouri, in neutral and stable atmosphere. *U.S. EPA Res.* no. EPA-450/3-75-066, Res. Tri. Pk., NC.

LIU, H. T. & LIN, J. T. 1976 Plume dispersion in stably stratified flows over complex terrain; Phase 2. *U.S. EPA Env. Monitoring Ser. Rep.* no. EPA-600/4-76-022. Res. Tri. Pk., NC.

LONG, R. R. 1955 Some aspects of the flow of stratified flows. III. Continuous density gradients. *Tellus* **7**, 342–357.

LONG, R. R. 1972 Finite amplitude disturbances in the flow of inviscid rotating and stratified fluids over obstacles. *Ann. Rev. Fluid Mech.* **4**, 69–92.

MARWITZ, J. D., VEAL, D. L., AUER, A. H. & MIDDLETON, J. R. 1969 Prediction and verification of the air flow over a three-dimensional mountain. *Natural Resources Res. Inst. Tech. Rep.* no. 60. University of Wyo.

MILNE-THOMPSON, L. M. 1960 *Theoretical Hydrodynamics*, 4th ed. Macmillan.

OSTER, G. & YAMAMOTO, M. 1963 Density gradient techniques. *Chem. Rev.* **63**, 257–268.

PAO, Y. H., LIN, J. T., CARLSEN, R. L. & SMITHMEYER, L. P. C. 1971 The design and construction of a stratified towing tank with an oil-lubricated carriage. *Flow Res. Rep.* no. 4, Flow Res., Kent, Wash.

QUENEY, P., CORBY, G. A., GERBIER, N., KOSCHMIEDER, H. & ZIEREP, J. 1960 The airflow over mountains. *World Met. Org. Tech. Note* no. **34**. Geneva, Switz.

RILEY, J. J., LIU, H. T. & GELLER, E. W. 1976 A numerical and experimental study of stably stratified flow around complex terrain. *U.S. EPA Env. Monitoring Ser. Rep.* no. EPA-600/4-76-021. Res. Tri. Pk., NC.

SCHRAUB, F. A., KLINE, S. J., HENRY, J., RUNSTADLER, P. W. & LITTEL, A. 1965 *Basic Engng* **87**, 429–444.

SCORER, R. S. 1954 Theory of airflow over mountains, III: Air stream characteristics. *Quart. J. Roy. Met. Soc.* **80**, 417–428.

SCORER, R. S. 1968 *Air Pollution*. Pergamon.

SNYDER, W. H., 1979 The EPA meteorological wind tunnel; its design, construction and operating characteristics. *U.S. EPA Env. Mon. Ser. Rep.* EPA 600/4-79-051, RG. Tri. Pk, N.C.

SNYDER, W. H., BRITTER, R. E. & HUNT, J. C. R. 1979 A fluid modelling study of the flow structure and plume impingement on a three dimensional hill in stably stratified flow. *Proc. 5th Int. Conf. on Wind Engng, Fort Collins.* Pergamon.

SYKES, R. I. 1978 Stratification effects in boundary layer flow over hills. *Proc. Roy. Soc.* A **361**, 225.

THOMPSON, R. S. & SNYDER, W. H. 1976 EPA fluid modeling facility. *Proc. Conf. on Envir. Modeling and Simulation, Cincinnati, Ohio.* EPA-600/9-76-016. U.S. Environmental Protection Agency, Washington, D.C.

TURNER, J. S. 1973 *Buoyancy Effects in Fluids.* Cambridge University Press.

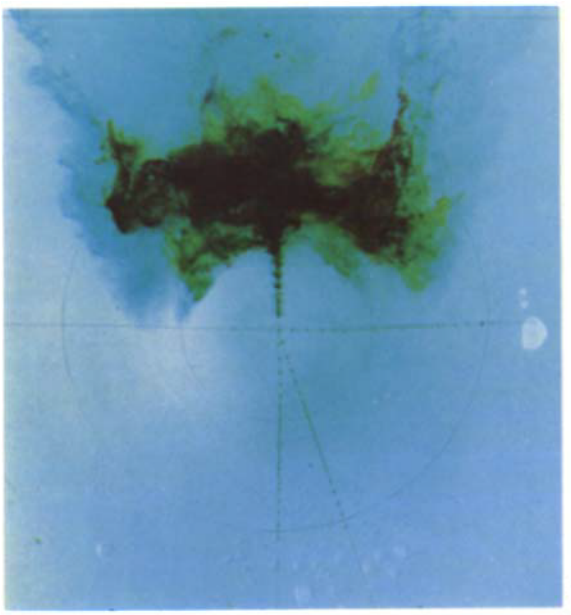

(*c*)

(*d*)

(*a*)

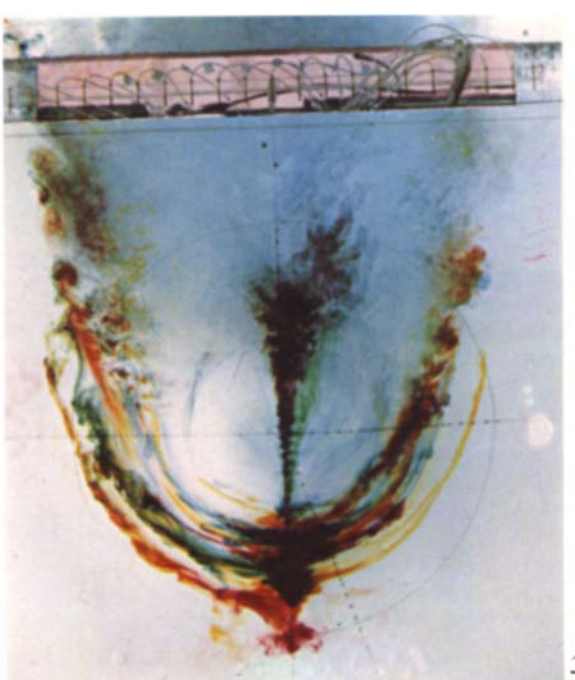

(*b*)

FIGURE 8 (*a–d*). See plate 2 for the legend.

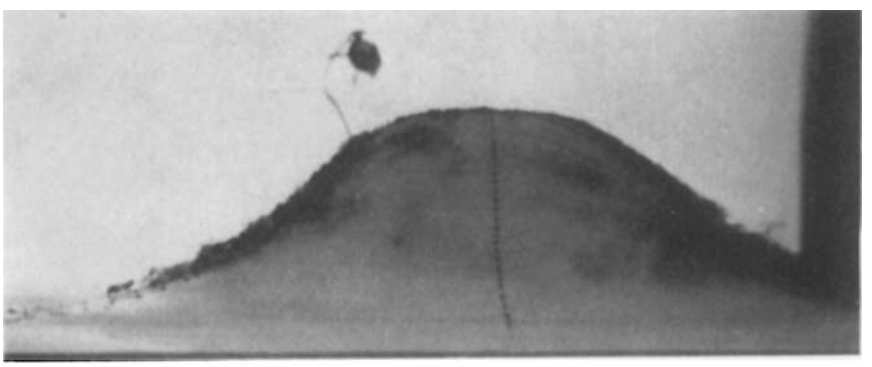

(*e*)

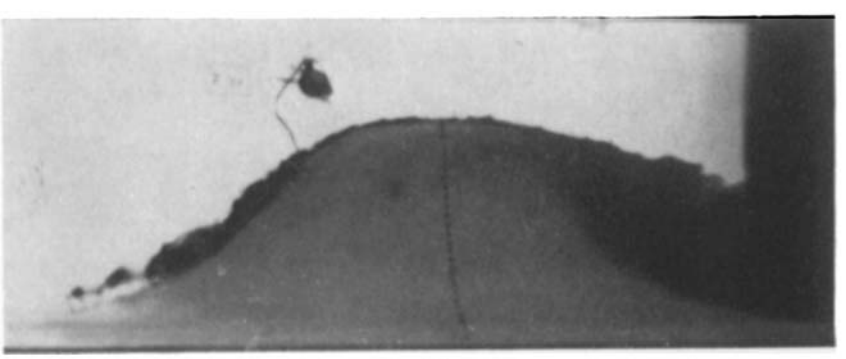

(*f*)

FIGURE 8. Visualization of surface flow patterns from injection of tracers. (*a*) Dye release from 180° ports, $F = 0{\cdot}2$, side view. (*b*) Dye release from 180° ports, $F = 0{\cdot}2$, top view. (*c*) Dye release from 0° ports, $F = 0{\cdot}2$, top view. (*d*) Dye release from 180° ports, $F = 0{\cdot}4$, side view. (*e*) Dye release from 180° ports, $F = 0{\cdot}9$, side view. (*f*) Dye release from 180° ports, $F = 1{\cdot}6$, side view.

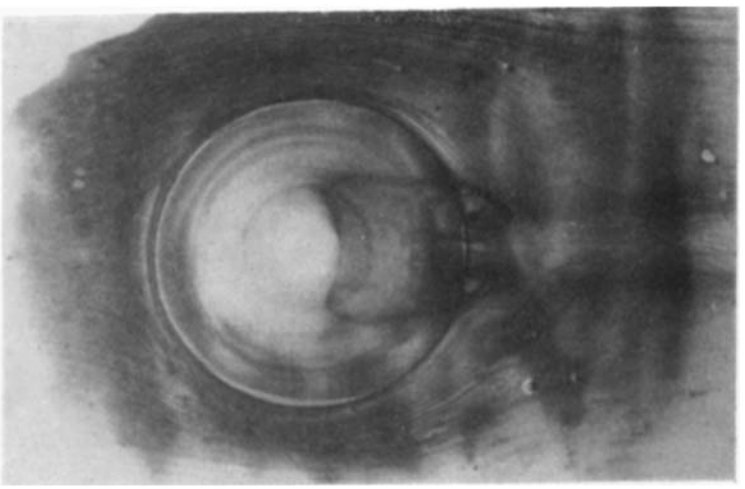

(*c*)

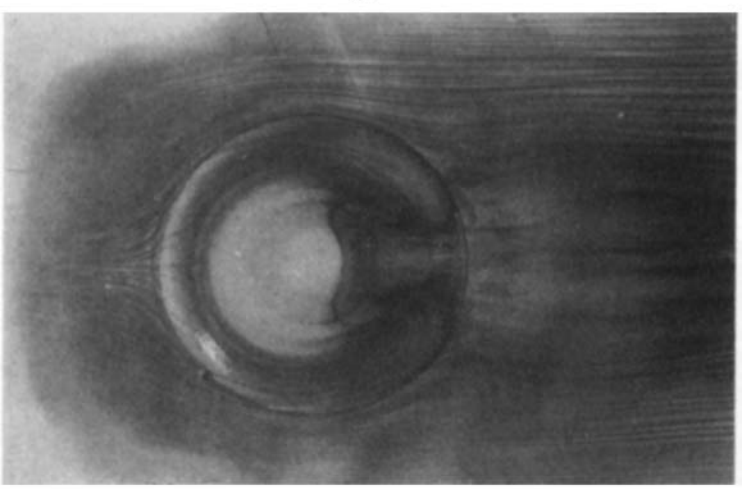

(*d*)

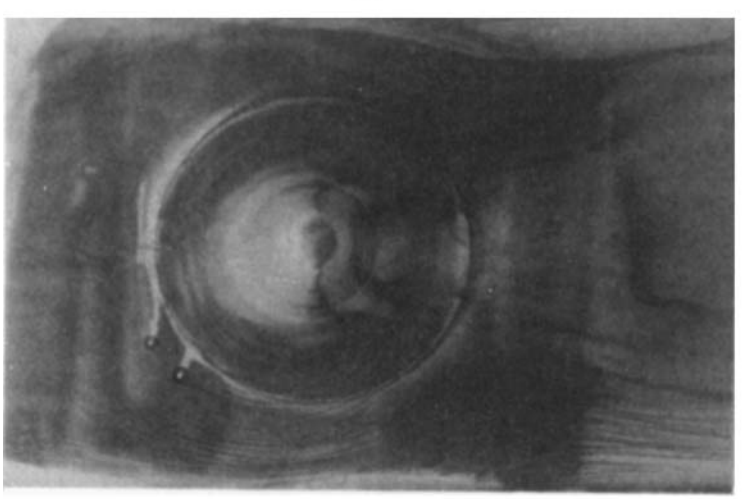

(*e*)

FIGURE 9 (*c, d, e*). Visualization of surface shear stress patterns. Top views of gelatin/dye in small tank. $F = 0{\cdot}4$, $1{\cdot}0$, ∞, and $Re = 400$, 800, 1000, respectively.

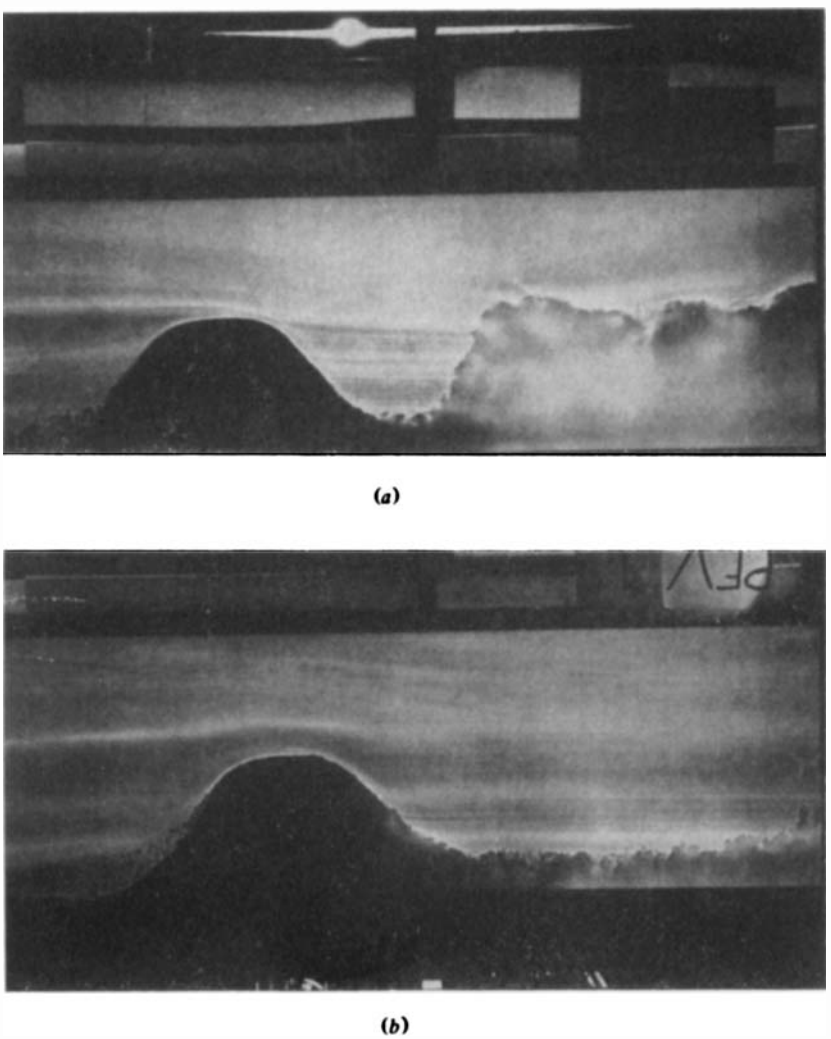

(*a*)

(*b*)

FIGURE 10. Shadowgraphs of flow over hill ($N = 1{\cdot}33$ rad s^{-1}). (*a*) $F = 0{\cdot}6$, $Re = 41\,200$. (*b*) $F = 1{\cdot}0$, $Re = 68\,700$.